AGU PUBLICATIONS

Tectonics

RESEARCH ARTICLE
10.1002/2014TC003647

Key Points:
- Oligocene-Miocene Ayaviri basin governed by basin margin thrusting
- Timing of basin margin thrusting constrained by newly dated growth strata
- Oligocene to mid-Miocene northern Altiplano tectonics driven by shortening

Supporting Information:
- Readme
- Figure S1
- Figure S2
- Table S1

Correspondence to:
N. D. Perez,
nicholas.d.perez@utexas.edu

Citation:
Perez, N. D., and B. K. Horton (2014), Oligocene-Miocene deformational and depositional history of the Andean hinterland basin in the northern Altiplano plateau, southern Peru, *Tectonics*, *33*, 1819–1847, doi:10.1002/2014TC003647.

Received 10 JUN 2014
Accepted 7 AUG 2014
Accepted article online 13 AUG 2014
Published online 29 SEP 2014
Corrected 28 SEP 2015

This article was corrected on 28 SEP 2015. See the end of the full text for details.

Oligocene-Miocene deformational and depositional history of the Andean hinterland basin in the northern Altiplano plateau, southern Peru

Nicholas D. Perez[1] and Brian K. Horton[1]

[1]Institute for Geophysics and Department of Geological Sciences, Jackson School of Geosciences, University of Texas, Austin, Texas, USA

Abstract Cenozoic basin fill of the northern Altiplano plateau records the tectonic development of the flanking Western Cordillera magmatic arc and Eastern Cordillera fold-thrust belt. The Ayaviri hinterland basin of southern Peru contains a ~2300 m thick succession of fluvial sandstones and overbank siltstones (upper Oligocene Puno Group and lower Miocene lower Tinajani Formation) capped by ~400 m of alluvial fan conglomerates (middle Miocene upper Tinajani Formation). New U-Pb zircon chronostratigraphic constraints from ~30 to 15 Ma yield sediment accumulation rates of 110–660 m/Myr. Newly dated growth strata highlight the genetic role played by thrust displacement in basin evolution. A several phase accumulation history derived from chronostratigraphic, provenance, and structural data reveals Oligocene basin filling by fluvial sand and mud that changes provenance from Western Cordillera Mesozoic-Cenozoic volcanic rocks to Paleozoic-Mesozoic Eastern Cordillera sedimentary rocks driven by deformation along the southwest directed, northeastern basin margin Ayaviri thrust at 28–26 Ma. Continued early Miocene fluvial deposition was sourced solely from the Eastern Cordillera. An abrupt middle Miocene shift to coarse alluvial fan deposition sourced from the Western Cordillera was driven by out-of-sequence deformation along the northeast directed, southwestern basin margin Pasani thrust at 18–16 Ma. This northern Altiplano out-of-sequence deformation was coincident with increased Eastern and Western Cordillera exhumation and thrusting and may be symptomatic of changes in critical wedge dynamics. The overall record of basin sedimentation and syndepositional fold-thrust deformation emphasizes the role of regional shortening in governing crustal thickening and basin evolution in the central Andes during the Oligocene to Miocene.

1. Introduction

The mechanisms responsible for the evolution of long-lived sedimentary basins in hinterland settings of convergent orogenic systems remain poorly constrained. Debate has centered on the establishment of internal drainage, partitioning, and coalescence of basin depocenters, modes of syndepositional deformation, and processes responsible for basin subsidence [*Jordan and Alonso*, 1987; *Allmendinger et al.*, 1997; *Tapponnier et al.*, 2001; *Sobel et al.*, 2003; *Carroll et al.*, 2010; *Horton*, 2012]. For example, hinterland basins of the Altiplano-Puna plateau have been variably interpreted as the product of thrust-related flexural subsidence, sediment ponding within internally drained topographic lows, or subsidence driven by strike-slip deformation [e.g., *Sempere et al.*, 1990; *Baby et al.*, 1990; *Vandervoort et al.*, 1995; *Rochat et al.*, 1999; *Horton et al.*, 2002; *Elger et al.*, 2005; *Rousse et al.*, 2005; *Carlotto*, 2013]. Successfully reconstructing the spatial and temporal history of these basins in the context of convergent margin dynamics remains a challenge, yet provides critical evidence for the history and style of deformation controlling the orogenic evolution of elevated hinterland regions.

In the central Andes (Figure 1), the Altiplano plateau preserves a series of internally drained hinterland basins in Bolivia and southern Peru containing up to ~12 km of synorogenic Cenozoic sediment [*Horton et al.*, 2001, 2002; *Carlotto*, 2013]. These nonmarine hinterland basins are a key recorder of the tectonic processes that controlled Altiplano development throughout the Cenozoic. Although unconformable relationships within the stratigraphic record have long been used to propose multiple separate pulses of deformation with intervening periods of quiescence [e.g., *Steinmann*, 1929; *Megard et al.*, 1984; *Ellison et al.*, 1989; *Noblet et al.*, 1996], most syntheses of available depositional records demonstrate continuous, long-lived subsidence and sedimentation in the Cenozoic basins of the central Andean hinterland [*Jordan and Alonso*, 1987; *Allmendinger et al.*, 1997; *Horton*, 2012; *Carlotto*, 2013].

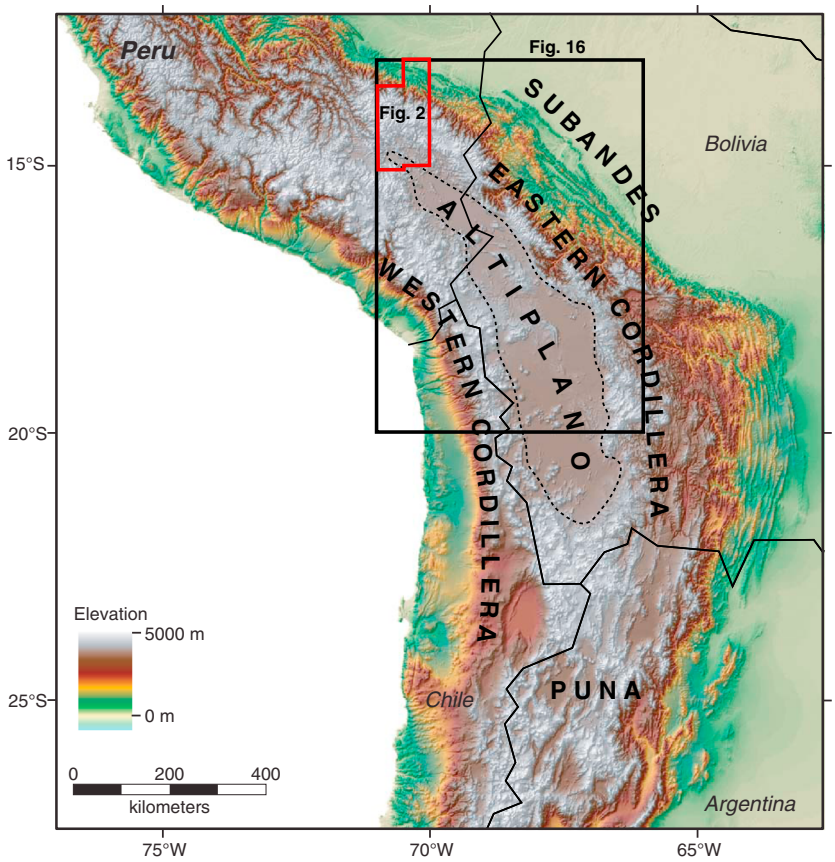

Figure 1. Topographic map of the central Andes (after *Garzione et al.* [2014]) showing the southern Peruvian study area (thick red outline, Figure 2; thick black outline, Figure 16), situated at the northern tip of Altiplano. Study area encompasses Altiplano, Eastern Cordillera, and Subandes.

Hinterland basins have also been used to define the history of surface uplift in the Altiplano. Significant debate persists over the apparently heterogeneous and localized surface uplift events that postdate most Andean shortening. Rapid uplift events have been proposed for the Altiplano of Bolivia (~10–6 Ma [*Garzione et al.*, 2006]), Eastern Cordillera of Bolivia (after 12–9 Ma [*Barke and Lamb*, 2006] and 24–15 Ma [*Leier et al.*, 2013]), and Western Cordillera of Peru (~19–16 Ma [*Saylor and Horton*, 2014]) based on paleoaltimetric and canyon incision proxies. Many studies have called on foundering or delamination of continental lithosphere as a potential mechanism to explain rapid high-magnitude surface uplift events throughout the central Andes [*Kay and Kay*, 1993; *Garzione et al.*, 2006; *DeCelles et al.*, 2009], although some regions retain subcrustal lithosphere [*Beck and Zandt*, 2002]. Improved records of upper crustal shortening are needed in localities with accompanying paleoaltimetric studies to evaluate the links between the timing and magnitude of deformation and the onset of surface uplift.

Key questions remain regarding the timing and style of deformation across the central Andes despite long-lived depositional records. It remains unclear whether the central (Bolivian) and northern (Peruvian) Altiplano structural systems are linked by a shared history of upper crustal deformation, including proposed major phases of thrust and strike-slip faulting. Existing timing constraints from the Eastern Cordillera in Bolivia and southern Peru suggest widespread Eocene cooling associated with advance of the deformation front [*Farrar et al.*, 1988; *Barnes et al.*, 2006; *Gillis et al.*, 2006; *Murray et al.*, 2010; *Leier et al.*, 2010; *Mosolf et al.*, 2011]. In Peru, the potential kinematic links between major structural features such as the Cordillera de Carabaya, central Andean backthrust belt, and Altiplano bounding structures (Pasani and Ayaviri faults) remain poorly constrained [*Sempere et al.*, 1990; *Sandeman et al.*, 1995; *Carlotto*, 2013]. Likewise, the potential broader links between deformation, deposition, and variations in slab processes are not well resolved. Using depositional and deformational records, some have argued for long-term Andean shortening that advanced

systematically toward the Amazonian craton [*Noblet et al.*, 1996; *DeCelles and Horton*, 2003; *McQuarrie et al.*, 2005], in contrast with previous studies arguing for short discrete phases of deformation with long intervening quiescent periods [e.g., *Sébrier et al.*, 1988; *Sempere et al.*, 1990]. Others have suggested that shortening was spatially distributed for protracted periods of time, progressed irregularly or out of sequence, potentially due to an inherited crustal framework [*Oncken et al.*, 2006; *Hongn et al.*, 2007; *Mortimer et al.*, 2007; *Strecker et al.*, 2009]. Still, others have attributed major shortening events to punctuated shifts in the dynamics of the subducting slab [*Jordan et al.*, 1983; *Sandeman et al.*, 1995; *James and Sacks*, 1999]. Regardless, shortening plays a key role in the construction of the Altiplano [*Isacks*, 1988]. Comparing the shortening history of Peru and Bolivia will help assess whether deformation in the central Andes was part of a widespread organized structural system or accommodated by a collection of independent disconnected zones.

This study provides an improved record of northern Altiplano deposition from the Ayaviri basin and precise age constraints on the timing and nature of Cenozoic upper crustal deformation in the Andean hinterland. We use new sedimentological, structural, and geochronologic data sets to define the history of sediment accumulation, timing and style of basin-controlling structures, and sedimentary response to changes in Andean tectonics in southern Peru. Finally, we highlight important similarities in structure and basin style spanning southern Peru and Bolivia, suggesting potential regional links between the deformation and subsidence history across the Altiplano.

2. Geologic Background

The central Andean (Altiplano-Puna) plateau (Figure 1) spans the elevated hinterland regions of southern Peru, Bolivia, and northern Argentina at an average elevation of ~3.7 km [*Isacks*, 1988; *Allmendinger et al.*, 1997]. This high topography is the result of long-lived crustal shortening along the convergent margin of western South America [*Coira et al.*, 1982], and crustal thickening may rely on magmatic addition [*Kay and Coira*, 2009], removal of lower lithosphere [*Beck and Zandt*, 2002], or crustal flow [*Husson and Sempere*, 2003]. The central Andes have experienced the greatest shortening within the orogenic belt, with over 300 km of margin-perpendicular shortening [*Kley and Monaldi*, 1998; *McQuarrie*, 2002]. Cenozoic hinterland basins preserved within the Altiplano contain the sedimentary record of Andean orogenesis. The position of these hinterland basins, situated between the volcanic arc (Western Cordillera) and retroarc fold-thrust belt (Eastern Cordillera/Subandes), highlights their role as a major repository of the erosional products of Andean volcanism and shortening (Figure 2).

The geologic history of southern Peru is highlighted by the main tectonic features defining the central Andes at 13–15°S (Figure 2). The Western Cordillera has been the locus of significant, generally continuous volcanic activity since the Late Cretaceous. The position of the magmatic arc has migrated across the western margin throughout the Cenozoic, at times overlapping the northernmost Altiplano [*Mamani et al.*, 2010]. The Eastern Cordillera of southern Peru contains the central Andean backthrust belt defined by generally southwest verging fold-thrust structures dominated by Cretaceous marine sandstones and limestones [*Sempere et al.*, 1990]. To the northeast of the backthrust belt is the Cordillera de Carabaya and Cordillera Real in Bolivia, northwest striking ranges composed largely of Triassic and middle to late Cenozoic igneous rocks [*McBride et al.*, 1983; *Farrar et al.*, 1988; *Kontak et al.*, 1990; *Sandeman et al.*, 1995]. Between the backthrust belt and the Cordillera de Carabaya is a region of noncoaxially deformed, middle to upper Paleozoic strata with fold and fault orientations that deviate from the regional tectonic strike of Andean structures. These orientations have been attributed to probable late Paleozoic deformation [*Mégard et al.*, 1971; *Laubacher*, 1978; *Dalmayrac et al.*, 1980; *Clark et al.*, 1990] prior to Andean shortening and are overlapped by a series of Miocene-Pliocene ash flow tuffs (the Macusani volcanic rocks) notable for their magmatic andalusite, muscovite, and high Al_2O_3 [*Laubacher*, 1978; *Pichavant et al.*, 1988; *Sandeman et al.*, 1995]. The southern Peruvian fore arc, Western Cordillera, and Eastern Cordillera have experienced significant counterclockwise vertical axis rotations that accommodated oroclinal bending, suggesting that strike-slip faulting, in addition to shortening, may have played a key role in central Andean tectonics [*Rousse et al.*, 2002, 2003; *Gilder et al.*, 2003; *Roperch et al.*, 2006].

Despite the unique position and large areal distribution of the Andean hinterland basins, the complete Cenozoic history and structures controlling many of these basins remain unclear. Previous studies of

Figure 2. Regional geologic map (after *INGEMMET* [1999], this study) across the Western Cordillera, Altiplano, Eastern Cordillera (including the Cordillera de Carabaya and Backthrust belt), and Subandean Zone showing major thrust faults and Ayaviri study area (black dashed box; Figure 3). Black stars with corresponding labels (listing depositional age and stratigraphic unit) denote locations of five U-Pb detrital zircon samples from Mesozoic and Paleozoic units used to characterize potential sediment sources for Cenozoic basin fill (Figure 9).

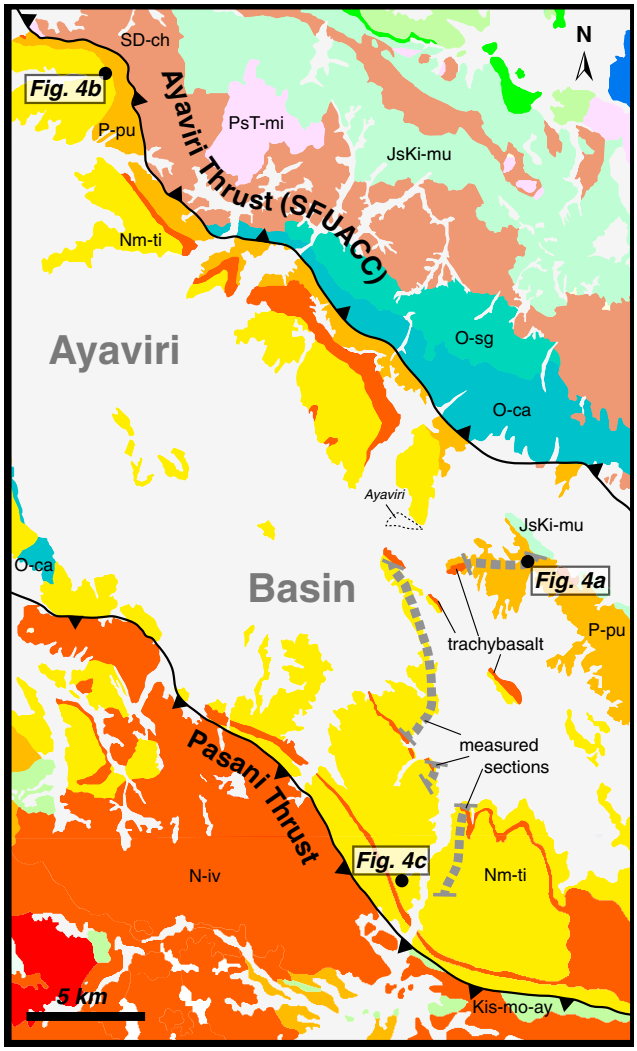

Figure 3. Simplified geologic map of the Ayaviri basin (after *INGEMMET* [1999], this study) showing the principal stratigraphic units (same key as Figure 2), the basin-bounding Ayaviri and Pasani thrusts, locations of growth strata outcrops and accompanying photos (Figure 4), and locations of measured sections (thick dashed gray lines with horizontal end caps).

hinterland basins in Bolivia [*Horton et al.*, 2001, 2002; *Hampton and Horton*, 2007; *Leier et al.*, 2010; *Murray et al.*, 2010; *Horton*, 2012] conclude that upper crustal shortening largely dictated basin genesis and the establishment of a plateau morphology in the central Altiplano. These studies posit that an early foreland basin was partitioned into a hinterland basin and subsequent Subandean foreland basin during large-scale eastward advance of deformation [e.g., *Roeder and Chamberlain*, 1995; *DeCelles and Horton*, 2003; *McQuarrie et al.*, 2005; *Siks and Horton*, 2011]. In contrast, studies of Altiplano basins in southern Peru suggest that Cenozoic basin evolution was localized and largely controlled by strike-slip faulting [*Carlotto*, 2013].

The Ayaviri hinterland basin in southern Peru occupies the narrow, northern tip of the Altiplano, where the flanking Eastern and Western Cordillera are in close proximity (Figures 2 and 3). In contrast to the north-south tectonic strike defining most of the Andean orogenic belt, the southern Peruvian segment is defined by a northwest-southeast strike, paralleling the continental margin. The northwest striking structures bounding the Ayaviri basin also approximate the structural boundaries between the Altiplano and flanking Eastern Cordillera and Western Cordillera. The northeastern and southwestern basin margins are defined by the Ayaviri and Pasani faults, respectively. To the southwest of the Ayaviri basin, Cenozoic volcanic deposits limit exposures of the underlying Mesozoic and Paleozoic succession to local isolated windows. To the northeast, Cenozoic volcanic rocks are limited, with Eastern Cordillera exposures dominated by Paleozoic and Mesozoic metasedimentary and sedimentary units.

The Ayaviri basin consists of >5–10 km of Cenozoic nonmarine clastic fill that unconformably overlie a mixed marine and nonmarine section of deformed Cretaceous strata. A western zone near the towns of Macari and Llalli preserves 3–6 km of mostly Paleogene deposits, whereas ~2700 m of the latest Oligocene to Miocene deposits are preserved near the town of Ayaviri and in Tinajani Canyon [*LaTorre et al.*, 2004; *Rodriguez et al.*, 1999]. Complex spatial and temporal variations in the Cenozoic stratigraphic framework of southern Peru led *Carlotto* [2013] to refer to the Oligo-Miocene deposits studied here as the Tinajani basin, in contrast to *Rousse et al.* [2005] who retain the Ayaviri basin designation. Beneath the Cretaceous-Cenozoic cover is a panel of Paleozoic and Permo-Triassic rocks that are proposed to have been deposited and deformed during multiple pre-Andean events [*Newell*, 1949; *Mégard et al.*, 1971; *Laubacher*, 1978; *Martinez*, 1980; *Laubacher and Mégard*, 1985; *Sempere et al.*, 2002; *Jimenez et al.*, 2009].

The Oligo-Miocene fill of the Ayaviri basin consists of ~2700 m of Puno Group and Tinajani Formation that are dominated by sandstones, siltstones, and conglomerates with minor lacustrine carbonates. Previous Oligocene to middle Miocene age constraints for the succession were based on dates from two volcanic horizons. The lower volcanic interval has been referred to as the Monterino or Cerro Ocuro volcanic rocks dated between ~29 and 25 Ma [*Bonhomme et al.*, 1985; *Fornari et al.*, 2002]. Upsection, interbedded ignimbrites commonly referred to as the Ocuviri tuffs were dated between 17.5 ± 0.6 and 17.3 ± 0.1 Ma [*Flores and Rodriguez*, 1999; *Rodriguez et al.*, 1999; *Ibarra et al.*, 2004; *Rousse et al.*, 2005; *Carlotto*, 2013]. Previous attempts to improve the Ayaviri basin chronostratigraphy using magnetostratigraphic techniques were hampered by significant postdeformational and recent magnetization [*Rousse et al.*, 2005].

3. Basin Margin Structures

Previous and new mapping efforts for the Ayaviri basin and basin margin structures provide constraints on major structural elements associated with basin evolution [*Flores and Rodriguez*, 1999; *Rodriguez et al.*, 1999; *Ibarra et al.*, 2004; *Carlotto et al.*, 2005; *Rousse et al.*, 2005; *Carlotto*, 2013]. The northeastern basin margin is defined by the northeast dipping Ayaviri fault, which is part of a larger system of faults known as both the Urcos-Ayaviri-Copacabana-Coniri Fault System (SFUACC acronym in Spanish) [*Sempere et al.*, 1990] or the Cusco Vilcanota Fault System [*Carlier et al.*, 2005] and can be traced ~350 km from southern Peru to Bolivia. It forms the structural boundary between the Altiplano and the Eastern Cordillera backthrust belt. The fault juxtaposes Middle Ordovician strata against Oligocene Puno Group. Bedding orientations from the ~5–6 km thick panel of Ordovician through Devonian strata in the northeast fault block dip approximately 40–45° to the northeast, suggesting that the fault dips similarly to the northeast for several tens of kilometers along strike. Along strike, variable Paleozoic units in the northeastern hanging wall block are juxtaposed against the Oligocene Puno Group in the footwall of the Ayaviri fault. The largest stratigraphic separation of approximately 7 km is observed north of the town of Ayaviri. Along strike to the northwest, the stratigraphic separation decreases to approximately 3 km, where the Permian Mitu Group is juxtaposed against the Oligocene Puno Group. The southwestern basin margin is defined by the southwest dipping Pasani fault that places the Cretaceous Ayavacas Formation on the middle Miocene upper Tinajani Formation. The northwestern trace of the Pasani fault strikes northwest-southeast, but the fault changes along strike to a west-northwest/east-southeast orientation. Much of the southwestern hanging wall block of the Pasani fault is covered by Neogene volcanic and hypabyssal intrusive rocks. However, local exposures of Oligocene Puno Group below the volcanic cover demonstrate an anticline trending parallel to the trace of the Pasani fault in the hanging wall. Local exposures of Cretaceous Ayavacas Formation beneath the Neogene volcanic cover suggests that fault separation is approximately 4–5 km.

Both faults are associated with significant footwall growth synclines that parallel the fault trace for tens of kilometers. The Ayaviri fault exhibits a flat on ramp cutoff relationship, with northeast dipping Paleozoic rocks thrust onto a footwall syncline composed of southwest dipping, and locally overturned northeast dipping, strata of the Oligocene Puno Group. The folded Puno strata are consistently observed in the footwall of the Ayaviri fault for more than 45 km along strike. Fault cutoff relationships show a systematic decrease from 7 to 3 km of stratigraphic separation from southeast to northwest along strike of the Ayaviri fault, from Middle Ordovician strata to Permian strata thrust onto Oligocene strata, suggesting decreasing thrust displacement along strike and/or the presence of a lateral ramp at depth. Hanging wall cutoffs for the Ayaviri fault have been eroded. The Pasani fault exhibits a ramp on ramp cutoff relationship with 4–5 km of stratigraphic separation and a hanging wall anticline preserved in Oligocene Puno Group strata exposed beneath a Neogene volcanic cover. The footwall syncline and growth relationships persist for more than 30 km along strike on the Pasani fault.

On the southwestern side of the Ayaviri fault (northeast basin margin), coarse sandstones and siltstones of the Oligocene Puno Group have fanning stratal dip values that are characteristic of growth strata [*Shaw et al.*, 2004] (Figure 4). Individual beds of the stratigraphically lower pregrowth strata have the steepest dips ranging between 54° overturned to the northeast and 71° upright to the southwest. Each bed has laterally consistent dips along strike. In contrast, overlying beds within the growth strata panel have dips that range between 60 and 8° upright to the southwest. Along the northeastern side of the Pasani fault (southwest basin margin), cobble conglomerates of the middle Miocene upper Tinajani Formation preserve similar fanning

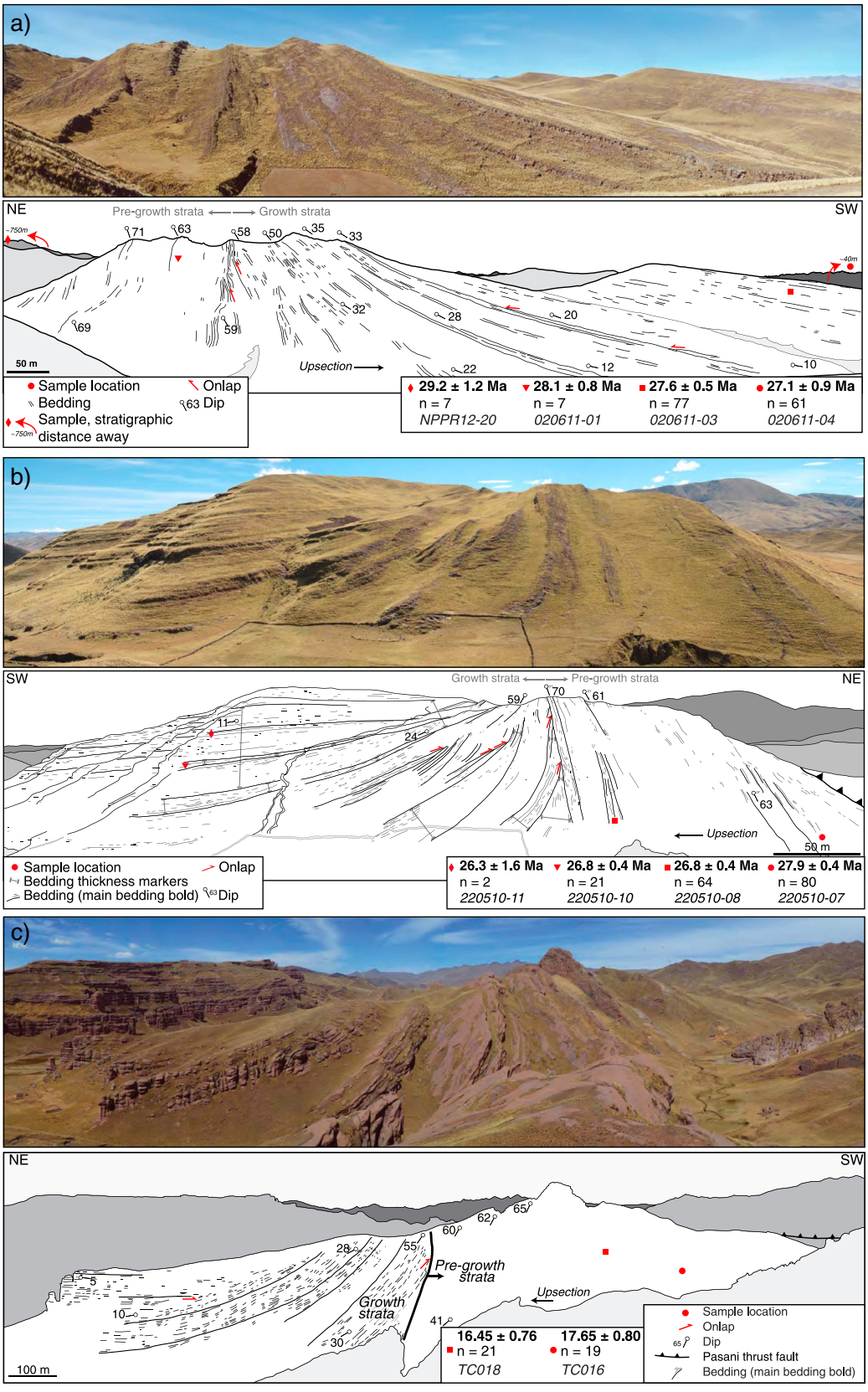

Figure 4. Three examples of growth strata preserved along the (a, b) Ayaviri fault and (c) Pasani fault. Ages from U-Pb zircon analyses of tuff or youngest detrital zircon population. Red symbols are sample locations.

dips. Individual beds within the pregrowth strata panel have laterally consistent dips that may vary between 70 and 40° upright to the northeast. Individual beds within the growth strata panel preserve dips that progressively vary between approximately 55° upright to the northeast and 5° upright to the southwest. Individual beds within both the Ayaviri and Pasani fault growth strata panels preserve progressive variation in dip over a lateral distance of a few hundred meters. Both sets of growth strata display upsection decreases in bedding dip and increased bedding flatness. The range of stratal dip variation is comparable to growth strata observed in the Pyrenees [*Riba*, 1976; *Anadón et al.*, 1986; *Ford et al.*, 1997].

Distinctive panels of recessive facies bounded by resistant sandstone beds within the growth strata along the Ayaviri fault can be traced laterally and consistently show thicknesses that increase away from the fault (Figure 4). Increases of the thickness of individual resistant sandstone beds are less apparent. The updip terminations of these recessive intervals may be truncated by an unconformity between the overlying and underlying resistant sandstone bed but are more often not observed due to erosion. Lateral thickness variations within the growth strata along the Pasani fault are difficult to observe within a single bed but are observed within intervals of cliff forming conglomerates and the intervening recessive units.

Multiple internal angular unconformities are associated with the footwall growth strata preserved along the Ayaviri and Pasani faults (Figure 4). Both growth strata locations along the Ayaviri fault (Figure 3) preserve one principal unconformity and multiple minor unconformities [*Ford et al.*, 1997; *Aschoff and Schmitt*, 2008]. The principal unconformity separates two stratigraphic units characterized by different geometries. The stratigraphically lower interval below the principal unconformity preserves dominantly tabular beds that have laterally consistent near-vertical dips and show no obvious internal angular unconformities. These are interpreted as pregrowth strata. The stratigraphically higher interval above the principal unconformity preserves beds that contain internal minor unconformities and represent growth strata. Angular variation across the principal unconformity varies between approximately 15° and 30°. The minor unconformities within the upper interval are dominantly low-angle (<5°) offlap relationships. Growth strata along the Pasani fault does not preserve a principal unconformity, and internal angular unconformities are rarely observed, potentially because of the coarse cobble conglomerates and thick bedding. The minor unconformities that are observed are less than approximately 10°.

The bedding geometries and angular unconformities within growth strata have been used to infer relative rates of uplift and sediment accumulation during active uplift and deformation of a structure as well as the style of fault or fold deformation. The prevalence of offlap geometries and a major unconformity with moderate angular discordance observed in growth strata along the Ayaviri fault is consistent with models suggesting that the relative rate of uplift in the hanging wall of the Ayaviri fault was greater than the sediment accumulation rate during the late Oligocene [*Anadòn et al.*, 1986; *Burbank and Verges*, 1994]. In contrast to the Ayaviri fault, the paucity of internal unconformities but prominent upsection decrease in bedding dip preserved in the growth strata along the Pasani fault may indicate that sediment accumulation rate outpaced local uplift of the hanging wall during the middle Miocene [*Aschoff and Schmitt*, 2008]. The lack of discrete dip domains within the growth strata panels along the Ayaviri and Pasani faults and the clear progressive dip variation along strike within individual beds suggests progressive limb rotation, rather than kink-band migration, was the dominant folding mechanism [*Suppe et al.*, 1992; *Zapata and Allmendinger*, 1996]. The geometries preserved in the growth strata along both faults are similar to models of fault propagation and trishear deformation [*Erslev*, 1991; *Ford et al.*, 1997].

4. Depositional Systems

The ~2700 m thick Oligocene-Miocene Puno Group and lower/upper Tinajani Formations [*Carlotto*, 2013] preserved in the Ayaviri basin (Figure 5) [*Flores and Rodriguez*, 1999; *Rousse et al.*, 2005] can be summarized as follows. The lower ~2300 m (Puno Group and lower Tinajani Formation) is interpreted as deposits of a sand-dominated braided and meandering fluvial system, characterized by high width to thickness ratios. The upper ~400 m (upper Tinajani Formation) is characterized by an abrupt change to thick pebble-boulder conglomerates representing sheetflood, debris flow, and streamflow deposition on an alluvial fan. Below are summaries of the key lithofacies, lithofacies assemblages, and interpreted depositional environments (Figures 6a–6j and Table 1). Despite changes in provenance and depositional environments, many of the deposits exhibit sheet-like geometries characteristic of other Altiplano basins [*Hampton and Horton*, 2007].

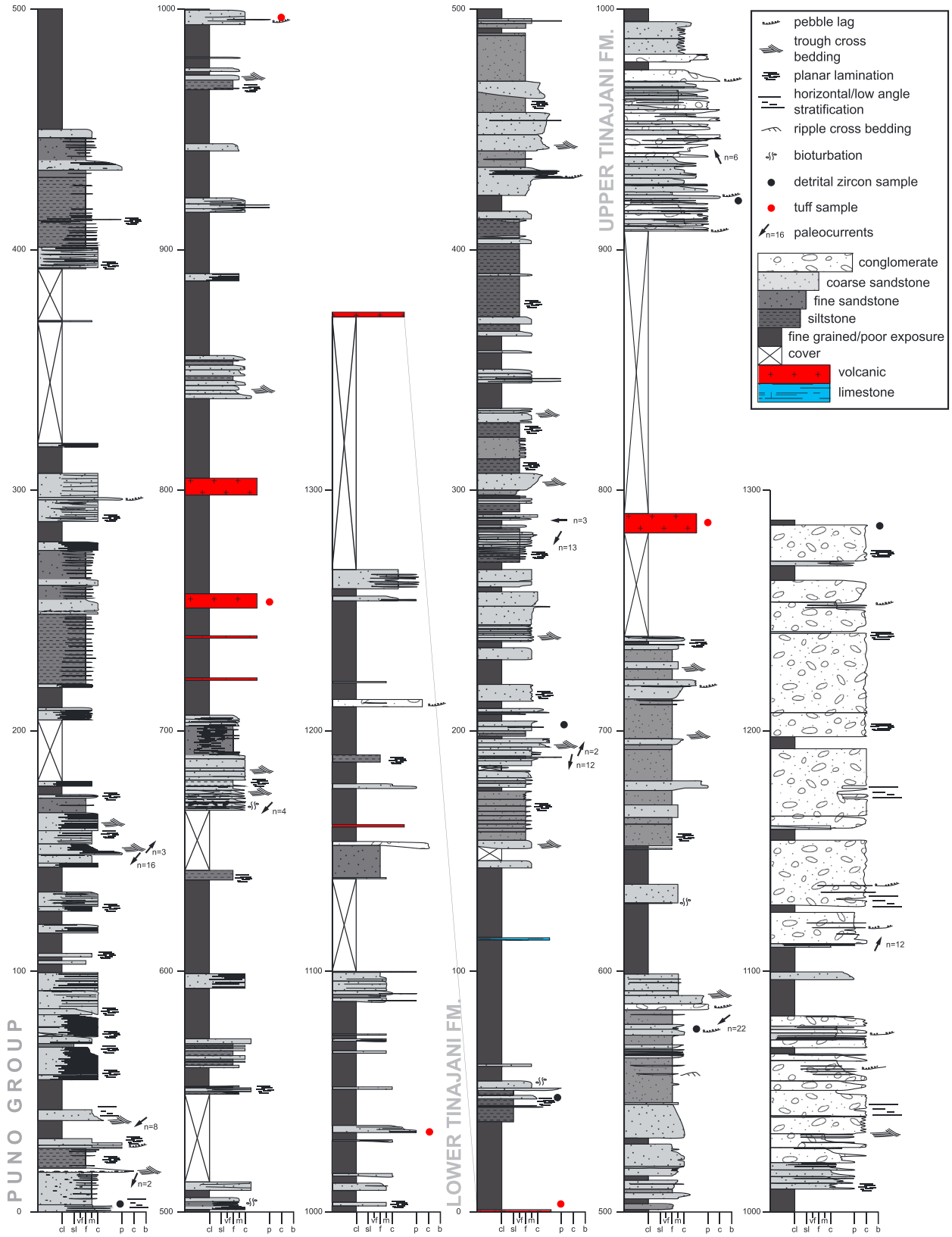

Figure 5. Composite-measured section showing lithofacies and sedimentary structures of the Ayaviri basin. The lower interval (section 1, Puno Group) disconformably overlies the Cretaceous Muni Formation east of Ayaviri. The upper interval (section 2, lower and upper Tinajani Formations) is conformable with underlying Puno Group, correlated by the trachybasalt flow.

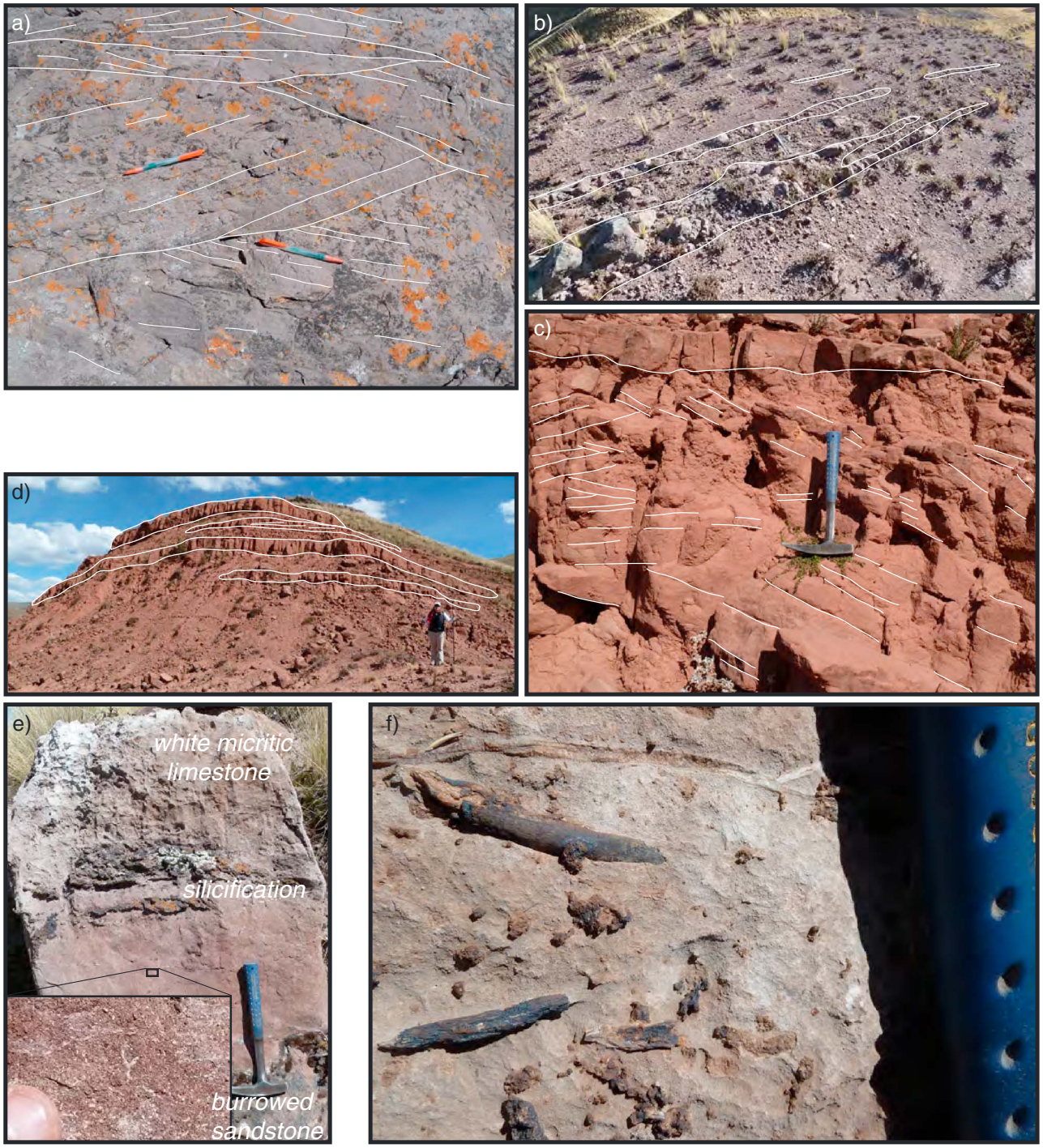

Figure 6. Photos of lithofacies and stratigraphic units from the lower ~2300 m sandstone-dominated section (Puno Group–lower Tinajani Formation, photos a–f) and upper ~400 m conglomeratic section (upper Tinajani Formation, photos g–j) of the Ayaviri basin. (a) Cross-stratified, medium- to coarse-grained lenticular sandstones interpreted as braided channel fill. Pens for scale. (b) Interbedded medium sandstones (white outline) and siltstones representing overbank deposits. Hammer for scale. (c) Planar cross-stratified fine- to medium-grained sandstones filling. (d) Anastomosing sandstone channels encased in fine siltstone. (e) Lacustrine deposits with gradational contact between red-brown burrowed sandstone below and white micritic limestone, separated by discontinuous chert. (f) Fossils preserved in limestone. (g) Cross-bedded coarse sandstone and pebble-boulder conglomerate interpreted as deposits in an alluvial fan setting. Person for scale. (h) Clast-supported pebble-boulder conglomerates from surging debris flow deposits. Note the sharp nonerosional base (white line) and multiple fining and coarsening upward cycles (denoted by white triangles). Jacob staff divisions are 10 cm. (i) Laterally continuous pebble-boulder conglomerate and coarse sandstone beds interpreted as sheetflood deposits on an alluvial fan. Person for scale. (j) Laterally continuous conglomerate and sandstone sheets of the upper Tinajani Formation exposed in Tinajani Canyon. For scale, river elevation ~3950 m, ridgetop elevation ~ 4210 m.

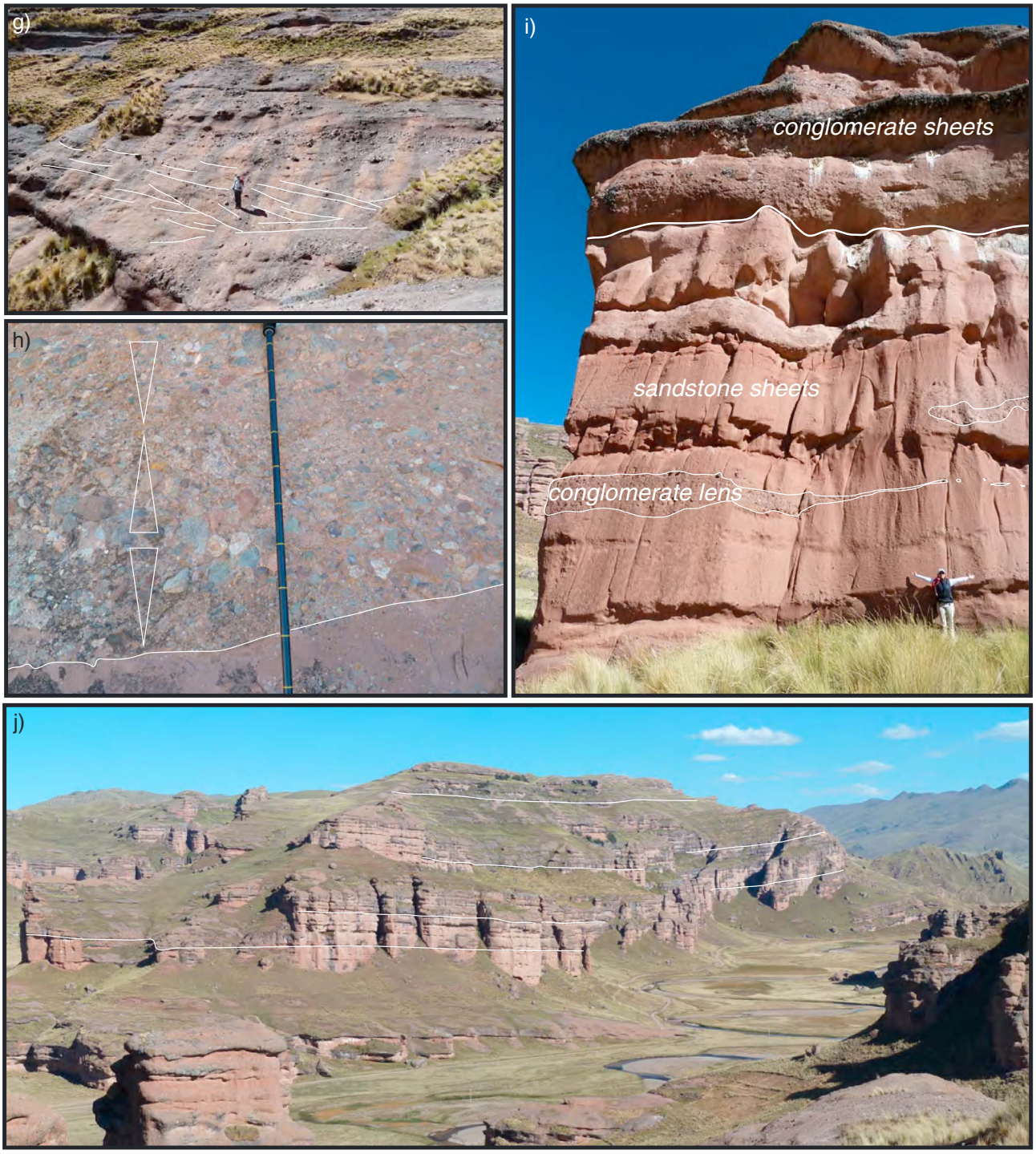

Figure 6. (continued)

4.1. Lower Section: Fluvial Channel and Floodplain Deposits

The lower ~2300 m is composed of numerous ~1–10 m thick upward fining intervals. Sandstones are typically tabular and laterally widespread (tens to hundreds of meters), with minor lenticular sandstones. Fine-grained intervals are poorly exposed, with limited carbonates and paleosol horizons. This lower section is interpreted to be deposited in a sand-dominated braided fluvial system transitioning upsection to isolated anastomosing channels with localized carbonate-producing lakes developed in overbank settings. The lower section also

Table 1. Facies Association and Interpretations for the Puno Group, Lower, and Upper Tinajani Formations

Facies Association	Lithofacies	Description	Interpretation
F1: Thinly interbedded mudstone, fine sandstone	Fl	Structureless, planar laminated, ripple-cross laminated, minor bioturbation, and soft sediment deformation; contains C1, S3	Fluvial overbank floodplain deposition
S1: Tabular medium, coarse sandstone	Sh, Sl, Sm, Sp, St	Structureless, subhorizontal, low-angle stratified sheet-like sandstone; lack scour; fine upward; isolated, dispersed pebbles; 0.5–2 m thick	Sandy braided river plain
S2: Lenticular medium, coarse sandstone	Sp, St, Ss, Gt	Associated with S1 facies; planar, trough-cross stratified sandstones; minor scouring; occasional basal pebble lag; lenticular profile; <1 m thick	Sandy channel fill with pebble lags in braided river
S3: Lenticular fine-medium sandstone	Sp	Lenticular, planar-cross stratified sandstone; encased in F1	Anastomosing river
S4: Cross-stratified coarse sandstone, pebble conglomerate	St, Gt, Sp, Gp	Well-organized trough-cross stratified coarse sandstone; pebble lag common; sharp base, top; 1–2 m scouring; lateral interfingering with G3	Coarse channel fill on alluvial fan
G1: Cross-stratified pebble conglomerates	Gp	>1 m tall planar-cross strata, lenticular profile contained within facies S1	Pebbly main channel fill in braided river
G2: Poorly bedded conglomerates	Gms, Gm	Disorganized; thickly bedded > 5 m; elevated coarse clasts at bed tops; diffuse or sharp bedding contacts; basal reverse grading; mostly no grain size trends; sometimes multiple upward coarsening, fining 5–10 cm cycles;	Surging debris flow on alluvial fan
G3: Sheet-like conglomerates and sandstones	Gm, Gh, Sh	Structureless, planar laminated, horizontally stratified thick sandstone, conglomerate couplet sheets; may fine or coarsen up; rare clast imbrication	Sheetflood on alluvial fan
C1: Thin carbonate, pedogenically altered sandstone	C, P, Fr	Bioturbated red marl grading upsection to structureless white micritic limestone; sharp-based carbonates interbedded with siltstones containing carbonated nodules	Ponded lacustrine and subaerially exposed floodplain

preserves growth strata (~750–1050 m level) associated with motion along the southwest directed Ayaviri backthrust (Figures 4a and 4b).

4.1.1. Tabular Sandstones (S1)

Tabular medium- to coarse-grained sandstones are common throughout the lower section. The subhorizontal to low-angle (<10°) stratified beds are 0.5–2 m thick, persist laterally for hundreds of meters and gradually taper and pinch out. These sheet sandstones often appear structureless but may contain planar or trough-cross laminations. Isolated and dispersed pebbles suggest dominantly sand with minor gravel bed load. Most sandstone packages lack significant basal scour and often fine upward. We interpret these laterally persistent, often structureless sandstones as longitudinal bars. *Miall* [1977] suggested that sediment transport in structureless braided fluvial bars occurred in planar sheets possibly at high flow regime. Overall, these tabular, sheet-like sandstones with high width to depth ratios are interpreted as braided fluvial deposits [*Smith*, 1974; *Miall*, 1977; *Rust*, 1978].

4.1.2. Lenticular Sandstones (S2)

Lenticular medium- to coarse-grained sandstones are less common but associated with the laterally persistent tabular sandstones described above. They are ~0.5–1 m thick, well-bedded, with planar to trough-cross stratification, lenticular profiles, and scoured bases with occasional basal pebble lags. The lack of lateral accretion surfaces and presence of lenticular geometries are consistent with channel fill in a braided fluvial system (Figure 6a) [*Miall*, 1977].

4.1.3. Interbedded Mudstones and Sandstones (F1)

Thinly interbedded mudstones and sandstones are common, occurring in ~0.5–10 m packages that are often poorly exposed and likely constitute most of the measured covered intervals. Where well exposed, the siltstones and mudstones show millimeter- to centimeter-scale planar and ripple-cross laminations with mud drapes, minor bioturbation, and minor small-scale soft-sediment deformation. Interbedded are thin (<0.2 m), lenticular, structureless, planar, and ripple laminated sandstones. Within the slope-forming mudstone intervals are 10 to 100 cm beds of massive carbonate mudstone and possible pedogenic horizons defined by

small calcrete nodule development, color mottling, and faint thin vertical features interpreted as possible root traces. Collectively, these intervals are interpreted as overbank deposits in broad fluvial floodplains with associated short-term lacustrine environments [*Miall*, 1977, 1978].

4.1.4. Carbonates (C1)

Thin carbonate and pedogenically altered sandstones are laterally restricted to less than a few hundred meters and commonly thinner than 1 m. They are preserved in association with overbank deposits. Carbonates lack lamination. Those with sharp bases are tabular in shape and found above fine sandstone and siltstones. Other carbonates may have diffuse bases, gradationally transitioning vertically over ~1 m thickness from structureless red-brown marly sandstone to pure carbonate (Figure 6e). Carbonates and associated sandstones may preserve thin, faint, lightly colored traces interpreted as bioturbation (Figure 6e, inset). The change from underlying burrowed red-brown sandstone below to white micritic limestone above may have a discontinuous, bedding parallel thin nodular chert layer. *Platt* [1989] interpreted similar deposits as ponded lacustrine environments in a distal floodplain. Silicification is interpreted as evidence for evaporative conditions. Carbonates are generally fossil poor macroscopically but preserve rare twigs (Figure 6f). Some structureless fine sandstones and siltstones within overbank deposits preserve mottled textures and vertically elongated carbonate nodules [*Leeder*, 1975; *Nijman and Puigdefabregas*, 1978]. These are interpreted as rhysoliths, and the lack of bedding is interpreted as a result of bioturbation. These zones themselves are interpreted as pedogenically altered, suggesting incipient soil formation and subaerial exposure. We interpret these beds as lacustrine deposits and pedogenic zones that developed in fluvial overbank and floodplain environments that experienced subaerial exposure and periodic inundation [*Miall*, 1978; *Platt*, 1989].

4.1.5. Isolated Lenticular Sandstones (S3)

Lenticular medium-grained sandstones are distinguished from the aforementioned lenticular sandstone facies by their isolated occurrence within siltstone-dominated intervals rather than an association with sheet-like sandstone bodies and the presence of numerous 10–30 cm thick cross stratification. These lenticular sandstones are typically observed near the top of the lower Tinajani Formation. The macroform of these sandstones encased in fine-grained intervals at first suggests isolated meandering channel bodies. However, the numerous inclined surfaces are different from the epsilon-shaped cross stratification typical of meandering streams [*Puigdefabregas and Van Vliet*, 1978]. These isolated channel bodies appear to have filled by dune migration, where the channels remained stationary until they were completely filled. We interpret these stationary channels lacking the hallmarks of meandering rivers as anastomosing rivers [*Nadon*, 1991; *Hampton and Horton*, 2007] (Figures 6c and 6d).

4.1.6. Lenticular Pebble Conglomerates (G1)

Cross-stratified pebble conglomerates are confined to the Puno Group at the base of the section. Pebbles are well rounded and commonly well organized along $>$1 m tall planar cross strata. They are lenticular in profile and interbedded or contained within the coarse-grained tabular sandstones facies (S1). Large-scale cross stratification suggests the passage of coarse gravel bars. We interpret these deposits as main channel body fill within a braided fluvial network [*Miall*, 1977, 1978].

4.2. Upper Section: Alluvial Fan Deposits

The ~400 m upper Tinajani Formation, exposed in Tinajani Canyon, contains substantially coarser material, including thick-bedded (1–5 m) cobble to boulder conglomerates interpreted as alluvial fan deposits. This upper interval preserves growth strata (~2300–2500 m level) associated with motion along the northeast directed Pasani fault.

4.2.1. Sheet-Like Sandstones (S4)

Cross-bedded coarse-grained sandstones and pebble conglomerates are well organized, with cross beds defined by pebble-cobble lags. Packages are well stratified with generally sharp bases and tops. Cross beds can be $>$ 1 m tall. Packages generally exhibit $>$ 1 m of scouring into underlying strata. Laterally, these deposits interfinger with planar-laminated or structureless thickly bedded sandstones and conglomerates with sheet-like geometries. These deposits are interpreted as incised channels filled with pebble lags on an alluvial fan (Figure 6g) [*Puigdefabregas and Van Vliet*, 1978; *Blair and McPherson*, 1994].

4.2.2. Disorganized Conglomerates (G2)

Disorganized, poorly bedded pebble-boulder conglomerates occur throughout the upper succession. Beds up to ~5 m thick may be either clast or matrix supported, with the largest clasts sometimes protruding

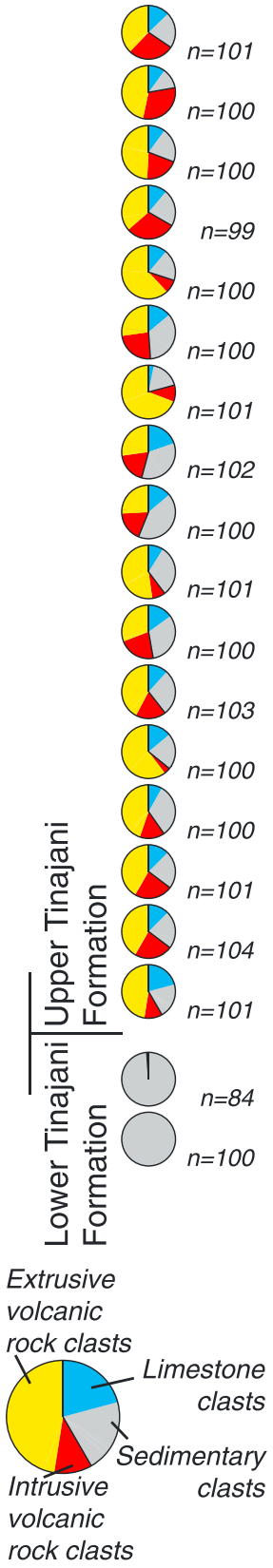

Figure 7. Clast count stations results. Note the change in clast composition between the lower and upper Tinajani Formation.

above the upper bed surfaces. Clasts are often poorly sorted, except along sharp basal contacts with limited or no scour that express thin zones of reverse grading and localized shear [*Nemec and Steel*, 1984]. Diffuse bedding contacts are common. Some individual packages contain multiple upward coarsening and fining cycles, suggesting amalgamation of multiple depositional events. Most show no grain size trend, but some may fine or coarsen upward. This facies is interpreted as debris flow deposits on a alluvial fan, with surging debris flows recording brief alternating periods of waning and intensified flow evidenced by multiple upward fining and coarsening variations in a single package (Figure 6h) [*Nemec and Steel*, 1984; *Blair and McPherson*, 1994; *Hartley et al.*, 2005].

4.2.3. Sheet-Like Conglomerates (G3)

Sheet-like pebble-boulder conglomerates and coarse-grained sandstones occur throughout the upper succession and are distinguished by their large lateral extent over 1000 m. They are up to ~5 m thick and are better organized than the aforementioned debris flow deposits and contain rare clast imbrication. Upper and lower bed contacts are commonly irregular and scoured with common internal horizontal stratification, although faint and poorly developed. The beds exhibit limited internal sorting and either fine or coarsen upward. Conglomeratic lenses within the larger sandstone sheets tend to display better developed cross bedding than surrounding beds [*Wells*, 1984]. These are similar to the gravel-sandstone couplets of *Blair and McPherson* [1994] and *Hartley et al.* [2005] interpreted as sheetflood deposits typical of alluvial fan environments (Figures 6i and 6j). These better organized conglomerates can be found in close association with the disorganized conglomerate (G2) facies, suggesting coexisting or alternating events of stream and debris flow processes.

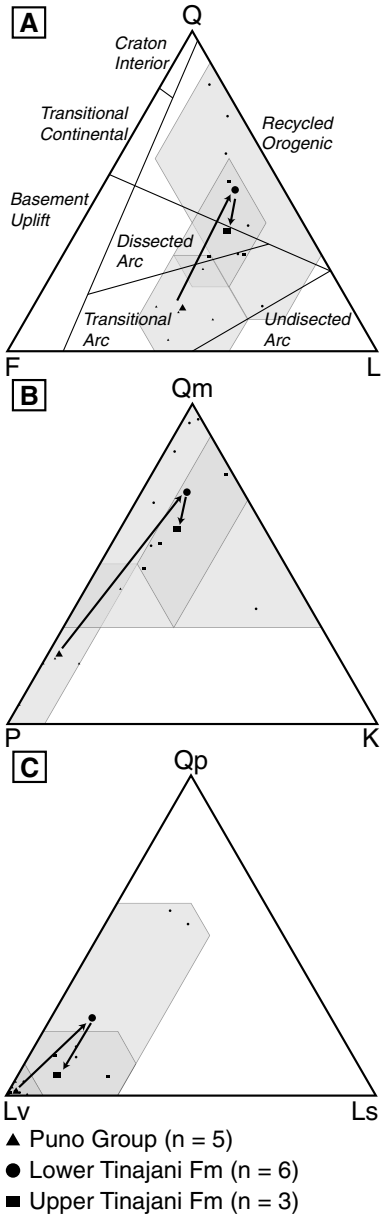

Figure 8. (a–c) Point count results from 14 thin sections from the Ayaviri basin. Provenance results reveal an upsection trend from transitional arc to recycled orogenic to dissected arc sources for the Puno Group, lower Tinajani Formation, and upper Tinajani Formation, respectively.

5. Sediment Provenance

5.1. Conglomerate Clast Compositions and Paleocurrents

Conglomerate clasts were counted at 19 stratigraphic levels throughout the upper ~1700 m of section (Figure 7). At lower levels, only two horizons in the lower Tinajani Formation contained sufficiently large clasts to identify clast lithologies. Both clast counts are dominated by sandstone, chert, siltstone, and quartzite lithologies, with only one volcanic clast observed. These lithologies are commonly observed in the Paleozoic succession exposed in the hanging wall of the Ayaviri thrust and other Paleozoic and Mesozoic units exposed in the Eastern Cordillera. Other isolated clasts or conglomeratic pebble lags observed throughout the section matched these clast count stations but lacked sufficient clasts ($n <$ 100) for a station. Paleocurrent measurements, although limited, show that the lower ~2.3 km of section (Puno Group and lower Tinajani Formation) had generally southwest directed paleoflow.

At higher levels, 17 clast counts for the conglomeratic upper Tinajani Formation (Figure 7) reveal a mix of extrusive, intrusive, limestone, and sedimentary rock clasts, in marked contrast to clast compositions of lower stratigraphic levels. Although no significant upsection trends are observed within the upper Tinajani Formation clast compositions, the igneous clasts are common throughout the Western Cordillera, and a local source of carbonate is present in mapped Cretaceous rocks in the proximal hanging wall of the Pasani thrust. The upper Tinajani Formation had very limited paleoflow indicators, but data suggest transport directed toward the north-northeast. Therefore, we interpret the upper Tinajani Formation shift in clast composition as evidence for a shift from Eastern Cordillera provenance to a dominant sediment source in the Western Cordillera.

The clast count and paleocurrent data suggest that the lower ~2.3 km of section was sourced from the Eastern Cordillera and transported generally toward the southwest. In contrast, the ~400 m upper Tinajani Formation conglomerates and paleocurrents suggest that sediment was sourced from the immediate Pasani fault hanging wall and Western Cordillera and transported generally toward the north.

5.2. Sandstone Petrographic Compositions

Fourteen petrographic thin section samples were analyzed using the Gazzi-Dickinson point-counting method to characterize the framework grain assemblage variability throughout the succession [*Dickinson and Suczek*, 1979]. Thin sections were stained for potassium and calcium feldspars. At least 300 sand grains (>0.0625 mm) per sample were counted.

Figure 8 shows the point count results for all 14 samples from the succession. Results are summarized in Table 2 and in three ternary diagrams: Q-F-L (total quartz, feldspar, and lithic grains; Figure 8a), Qm-P-K (monocrystalline quartz, calcium plagioclase, and potassium feldspar; Figure 8b), and Qp-Lv-Ls, (polycrystalline quartz, volcanic lithics, and sedimentary lithics; Figure 8c) (all diagrams after *Dickinson and Suczek* [1979]). Photomicrographs of the various observed lithic fragments are presented in the repository (Figure S1 in the supporting information). Results are shown for both individual samples and the average composition of each the Puno Group, lower Tinajani Formation, and upper Tinajani Formation. The average Puno Group composition ($Q_{13}F_{46}L_{41}$) is dominated by generally equal contributions of feldspars and lithic fragments, with subordinate quartz

Table 2. Thin Section Point Count Data for 14 Samples From the Ayaviri Basin

		Q F L %			Qm F Lt %			Qm P K %			Qp Lv Ls %		
Sample	Unit	Q	F	L	Qm	F	Lt	Qm	P	K	Qp	Lv	Ls
220510-03	Puno Group	12.27	47.58	40.15	12.27	47.58	40.15	20.50	77.02	2.48	0.00	94.39	5.61
220510-07	Puno Group	13.86	52.81	33.33	12.55	53.61	33.84	18.97	81.03	0.00	4.35	95.65	0.00
220510-08	Puno Group	3.64	54.64	41.72	3.64	54.64	41.72	6.25	93.75	0.00	0.00	100.00	0.00
220510-10	Puno Group	10.10	38.76	51.14	9.21	39.14	51.64	19.05	70.75	10.20	1.90	98.10	0.00
220510-11	Puno Group	25.66	34.21	40.13	25.17	34.44	40.40	42.22	48.33	9.44	1.65	96.69	1.65
240510-05	lower Tinajani Formation	14.11	23.93	61.96	13.58	24.07	62.35	36.07	14.75	49.18	1.01	95.96	3.03
TC034	lower Tinajani Formation	39.21	15.20	45.59	35.90	16.03	48.08	69.14	25.93	4.94	12.06	75.18	12.77
240510-08	lower Tinajani Formation	83.16	3.70	13.13	80.69	4.25	15.06	95.00	0.91	4.09	53.52	23.94	22.54
TC038	lower Tinajani Formation	30.37	22.39	47.24	28.84	22.88	48.28	55.76	33.33	10.91	4.38	93.13	2.50
240510-10	lower Tinajani Formation	73.31	3.72	22.97	68.53	4.38	27.09	93.99	3.83	2.19	57.69	26.92	15.38
TC045	lower Tinajani Formation	61.65	10.03	28.32	59.88	10.49	29.63	85.09	12.28	2.63	15.31	73.47	11.22
240510-13	upper Tinajani Formation	52.92	13.50	33.58	50.57	14.18	35.25	78.11	1.78	20.12	12.62	80.58	6.80
TC072	upper Tinajani Formation	29.50	30.75	39.75	29.28	30.84	39.88	48.70	38.86	12.44	0.79	99.21	0.00
TC076	upper Tinajani Formation	30.21	20.83	48.96	27.96	21.51	50.54	56.52	30.43	13.04	6.08	69.59	24.32

contributions, consistent with erosion of a transitional arc source. The average lower Tinajani Formation composition ($Q_{50}F_{13}L_{37}$) is consistent with a recycled orogenic source. It is typified by decreased contributions from feldspars. Quartz and lithic fragment content varies considerably throughout this formation, with compositions spanning recycled orogenic and arc sources. The average composition of the upper Tinajani Formation ($Q_{37}F_{22}L_{41}$) has a lithic fragment contribution similar to the Puno Group, yet has higher quartz contributions and lower feldspar contributions than the Puno Group. Sandstone compositions from the upper Tinajani Formation suggest erosion of a dissected arc.

6. U-Pb Geochronology

6.1. Methods

Zircon U-Pb results are presented for 23 samples to constrain both maximum depositional ages and sediment provenance, including 10 Cenozoic sandstones, eight volcanic tuffs from the Ayaviri basin and five Paleozoic-Mesozoic sandstones from the adjacent Eastern Cordillera. After crushing, water table, heavy liquid, and magnetic separation of zircon grains from the sandstones and tuffs, U-Pb geochronologic laser-ablation-multicollector inductively coupled plasma mass–spectrometry (LA-MC-ICPMS) analyses were conducted at the University of Arizona LaserChron center [*Gehrels*, 2000; *Gehrels et al.*, 2008].

Approximately 120 individual zircon grains ranging between 30 and 100 μm were randomly analyzed from each sandstone sample. Parts of grains with cracks or inclusions were not ablated. Sri Lankan zircon crystals with a known age of 564 ± 4 Ma (2σ error) were used as standards every fifth measurement to correct for intraelement and interelement fractionation. Resulting uncertainties were commonly 1–2% (2σ error) for both $^{206}Pb/^{238}U$ and $^{206}Pb/^{207}Pb$ ages. Additional details regarding methods for conducting analyses are presented by *Gehrels et al.* [2008]. Reported ages represent $^{206}Pb/^{238}U$ ages for zircon grains younger than 1000 Ma and $^{206}Pb/^{207}Pb$ ages for zircon grains older than 1000 Ma. Grain analyses with >30% discordance, >5% reverse discordance, or >10% uncertainty were discarded from further evaluation and interpretation.

6.2. U-Pb Detrital Zircon Provenance

6.2.1. Potential Zircon Sources

To characterize the potential detrital contributions from the Eastern Cordillera, we conducted LA-MC-ICPMS analyses of detrital zircon grains from five new sandstone samples representing Ordovician, Carboniferous, Permo-Triassic, and Cretaceous units (Figure 9). Although several key U-Pb age populations allow discrimination of potential zircon sources, other populations are nondiagnostic, as they are shared by multiple samples (e.g., ~1000 Ma Sunsas/Grenville), suggesting long-lived zircon grains and protracted sediment recycling throughout the Phanerozoic. Key age populations are highlighted: Cratonic (1500–2500 Ma), Sunsas/Grenville (900–1200 Ma), Pampean-Braziliano (500–700 Ma), Famatinian (400–500 Ma), Permo-Triassic (200–300 Ma), and Eocene-Cretaceous (50–150 Ma). Cratonic, Sunsas/Grenville, and Famatinian age populations are found in all samples. Famatinian zircons are found in all samples except the Ordovician San Gaban Formation (TC054).

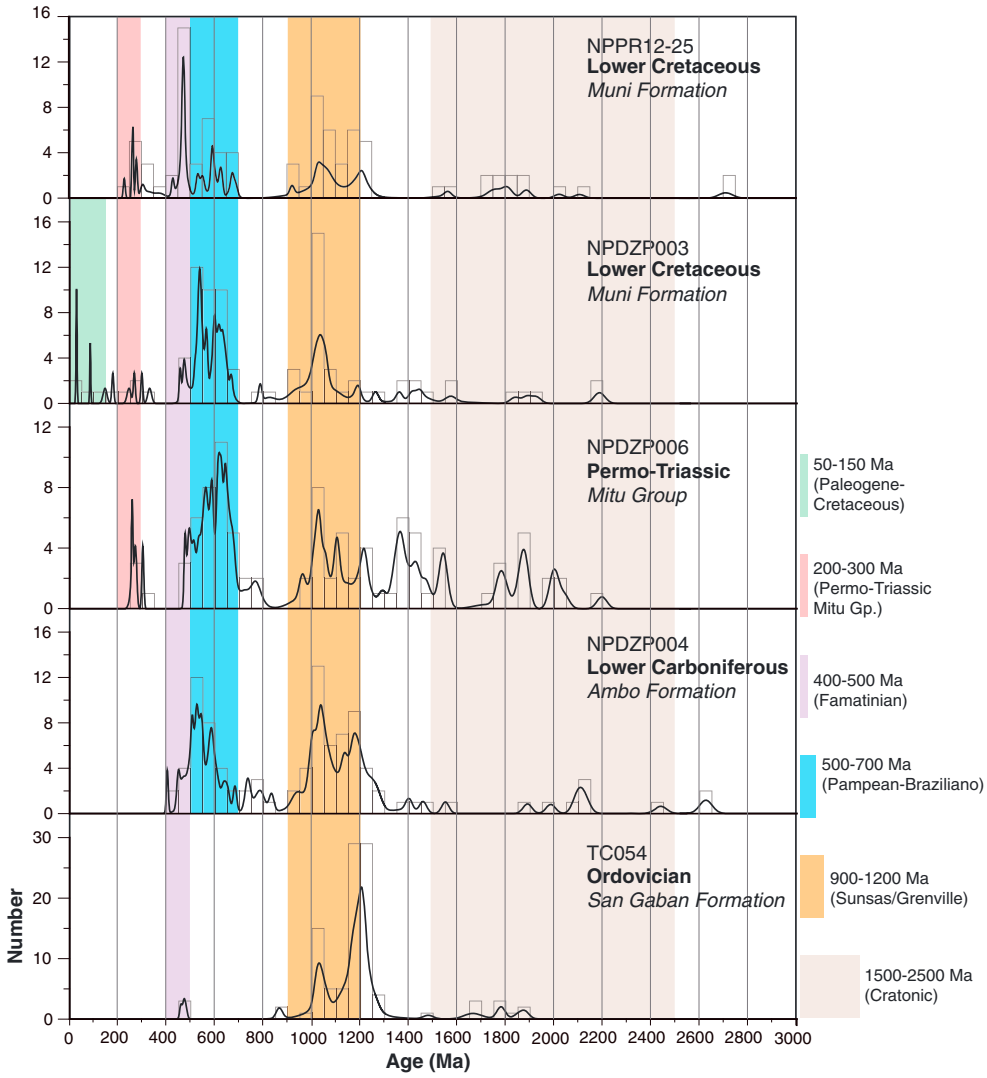

Figure 9. U-Pb age histograms (black bars) and probability density functions (black curves) depicting detrital zircon geochronologic results for five pre-Cenozoic sandstone samples from the Eastern Cordillera of southern Peru. Sample locations from Figure 2. Samples presented in stratigraphic order (oldest at base), with each histogram bin spanning 50 Myr and variable vertical axes based on number of zircon grains. Used to compare age spectra with Cenozoic Ayaviri basin detrital zircon samples shown in Figure 10. The presence of similar age populations in multiple samples suggests significant recycling. Note the paucity of Cretaceous zircons in the two Cretaceous samples.

Permo-Triassic zircons are found in the Permo-Triassic and both Cretaceous samples (NPDZP006, NPDZP003, and NPPR12-25). Cretaceous zircon populations are relatively rare in the source samples from the Eastern Cordillera, with $n = 3$ Cretaceous zircons for Cretaceous sample NPDZP003 and none for Cretaceous sample NPPR12-25.

6.2.2. Cenozoic Basin-Fill Samples

U-Pb results are presented for 10 Cenozoic sandstone samples from the Ayaviri basin (Figure 10). See Figure S2 for these samples displayed as kernel density estimation plots [*Vermeesch*, 2012]. The five lowest samples include NPPR12-20 from the base of the measured section (Figure 5), and four overlying samples (220510-07, 220510-08, 220510-10, and 220510-11) collected ~26 km along strike north of Ayaviri in growth strata along the Ayaviri back thrust (Figure 4). Stratigraphically above the trachybasalt flow at Cerro Ocuro (1372 m level in measured section, Figure 5; sample TC052 in Figure 11) are the upper five samples (240510-05, 240510-08, 240510-10, 240510-13, and TC076).

All of the Cenozoic sandstone samples contain contributions from Phanerozoic and Proterozoic zircon populations. Because samples 220510-07 and 220510-08 are dominated by Cenozoic zircons ($n > 70$) and

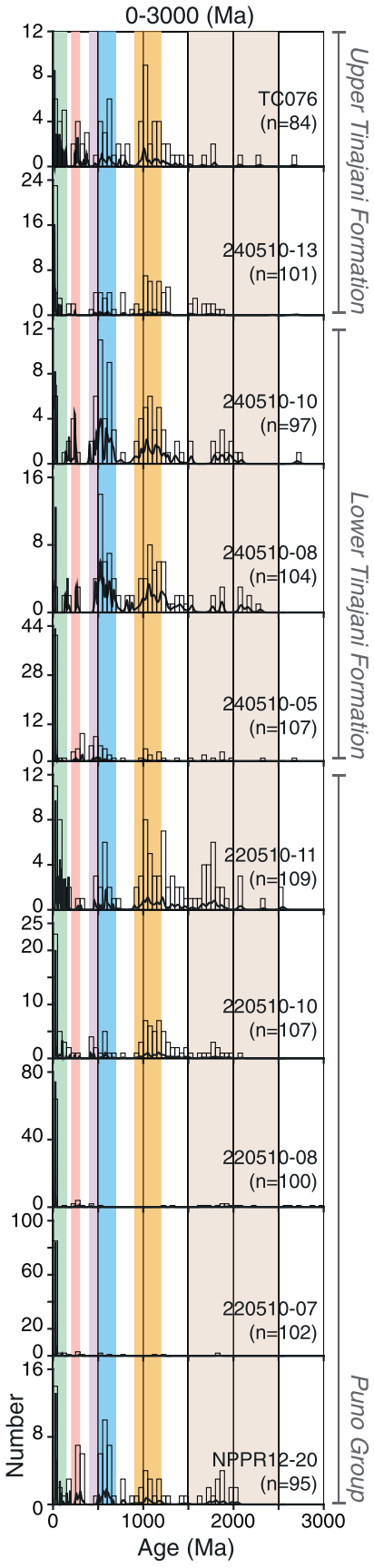

have limited ($n \leq 30$) pre-Cenozoic zircons, the associated provenance interpretations are made with caution as the statistical probability of representing all older zircon age populations in these two samples is relatively low [*Vermeesch*, 2004]. Several Precambrian to lower Paleozoic populations are present in nearly all basin-fill samples, including older cratonic ages (>1.2 Ga), Sunsas/Grenville ages (1–1.2 Ga), and Braziliano (~700 Ma) through Pampean ages (~500 Ma). Other populations, however, show significant variability among basin-fill samples, including Famatinian (400–500 Ma), Eocene-Cretaceous (50–150 Ma), and Cenozoic (50–15 Ma) populations. Upsection variations in detrital zircon age spectra provide insight into changes in sediment provenance associated with shifts in relative topography, drainage patterns, and/or basin architecture and are summarized below.

6.2.3. Cretaceous Zircons

Six of the 10 basin-fill samples from the Puno Group and upper Tinajani Formations have significant ($n \geq 3$) Cretaceous age populations (Figure 10). Such populations are relatively rare in the source samples from the Eastern Cordillera (Figure 9), with $n = 3$ Cretaceous zircons among both Cretaceous samples. Although limited Cretaceous intrusive units are found in the Eastern Cordillera, the most significant sources of Cretaceous zircons are volcanic-arc rocks of the Western Cordillera (e.g., Chocolate and Toquepala arcs [*Mamani et al.*, 2010]). We interpret the presence of Cretaceous zircons in the Puno Group and upper Tinajani Formation as evidence for delivery of sediment either from the Western Cordillera or reworked from Cenozoic deposits that have been eroded from the Eastern Cordillera.

6.2.4. Famatinian Zircons

Famatinian (~400–500 Ma) zircon populations are absent from the lowest two samples but are significant ($n > 3$) in the next seven samples and absent from the uppermost sample. *Bahlburg et al.* [2011] show that most Ordovician volcanic and sedimentary rocks in Peru are found in the Eastern Cordillera, as isolated Ordovician intrusions in the Arequipa Massif [*Loewy et al.*, 2004], or in the Marañon Massif [*Ramos*, 2009]. We interpret the appearance and persistence of this age population throughout deposition of the Puno Group, lower Tinajani Formation, and basal upper Tinajani Formation as evidence for likely delivery of sediment from the Paleozoic rocks found in the Eastern Cordillera which contain Famatinian zircons, from isolated Ordovician intrusions in the Arequipa Massif, or from Ordovician intrusions found in the Marañon Massif hundreds of kilometers to the northwest.

Figure 10. U-Pb age histograms (black bars) and probability density functions (black curves) depicting detrital zircon geochronologic results for 10 sandstone samples from Oligocene-Miocene fill of the Ayaviri basin. Samples presented in stratigraphic order (oldest at base), with each histogram bin spanning 50 Myr and variable vertical axes based on number of zircon grains. Color bars highlight the presence of age populations considered to be significant ($n \geq 3$ per histogram bin). Same color bar key as Figure 9.

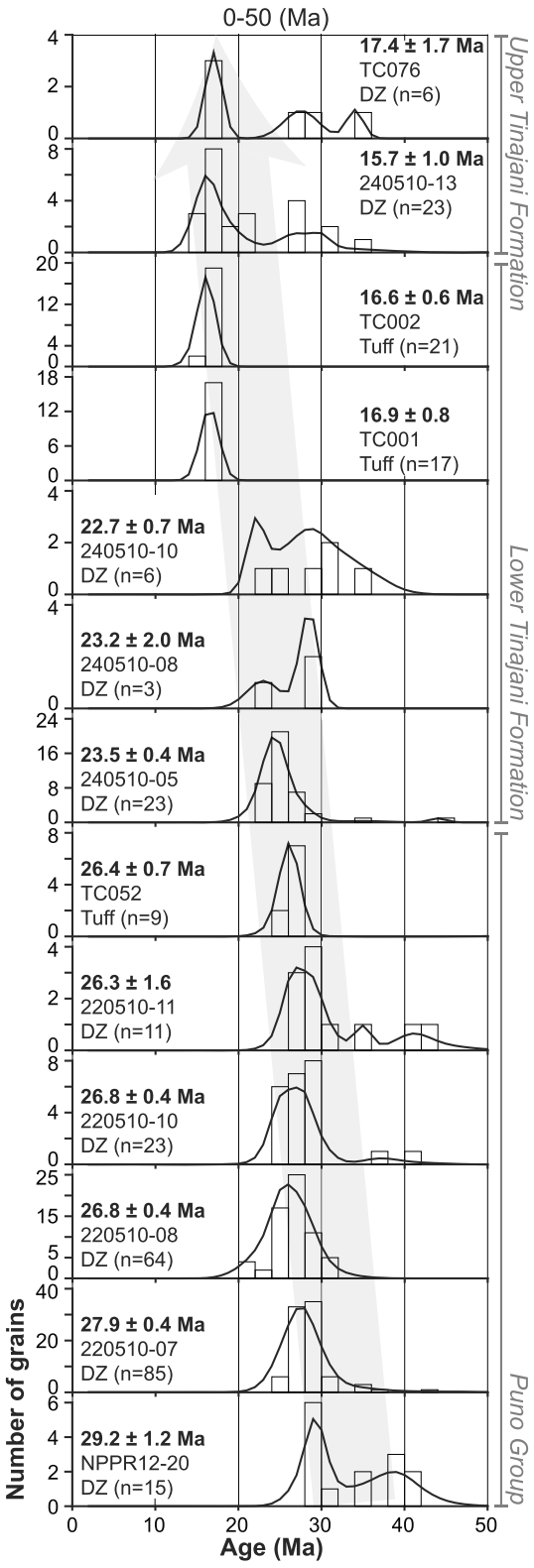

6.3. U-Pb Depositional Age Constraints

Continuous arc magmatism during the Cenozoic in southern Peru [*Mamani et al.*, 2010] suggests the potential for a steady supply of syndepositional volcanic zircons throughout the basin accumulation history. Accordingly, young zircon U-Pb ages are expected to be present in not only sampled tuffs but also in the detrital component of sampled sandstones. The U-Pb results (Figure 11) provide critical new geochronological constraints for the measured sections, including delineation of young detrital zircon age populations and volcanic tuff zircon populations. The following text highlights the important horizons for establishing the chronostratigraphic framework for the Ayaviri basin.

At the base of the measured section, ~30 m above the contact with the underlying Cretaceous Muni Formation, a sandstone sample (NPPR12-20) from the Puno Group yields a youngest zircon U-Pb age population of 29.6 ± 1.2 Ma (n = 15). At the ~750–1050 m levels are the three lowest samples of interbedded volcanic horizons found in the Puno Group within the Ayaviri back thrust growth strata east of Ayaviri (Figure 4a, Figure 3 location). These three volcanic ages are 28.06 ± 0.82 Ma, 27.56 ± 0.50 Ma, and 27.06 ± 0.88 Ma (samples 020611-01, 020611-03, and 020611-04, respectively). Four sandstone samples (220510-07, 220510-08, 220510-10, and 220510-11) from the equivalent growth strata succession exposed along strike north of Ayaviri, where volcanic horizons are absent (Figure 4b, Figure 3 location), demonstrate an upsection decrease in the youngest detrital age populations and agree with geochronologic constraints stratigraphically below, above, and along strike. At the 1372 m level, a trachybasalt flow at Cerro Ocuro south of Ayaviri, variably dated between 28.3 ± 1.0 and 26.9 ± 1.0 by *Bonhomme et al.* [1985],

Figure 11. U-Pb age histograms (black bars) and probability density functions (black curves) depicting geochronologic results (0–50 Ma) for all 10 detrital zircon ("DZ") sandstone samples and three interbedded volcanic ("Tuff") horizons from Oligocene-Miocene fill of the Ayaviri basin. Samples are depicted in stratigraphic order (oldest at base) with each histogram bin spanning 2 Myr. Sample labels provide the weighted mean age calculated for the youngest population of zircon grains, with the number (n) of analyzed grains ≥ 3. Four samples are from growth strata north of Ayaviri (Figure 4b; 220510-07, 220510-08, 220510-10, 220510-11); all other samples are from the measured section south of Ayaviri (Figure 5). Systematically decreasing ages upsection (highlighted by wide gray arrow) suggest that the youngest detrital zircon peaks may represent true depositional ages.

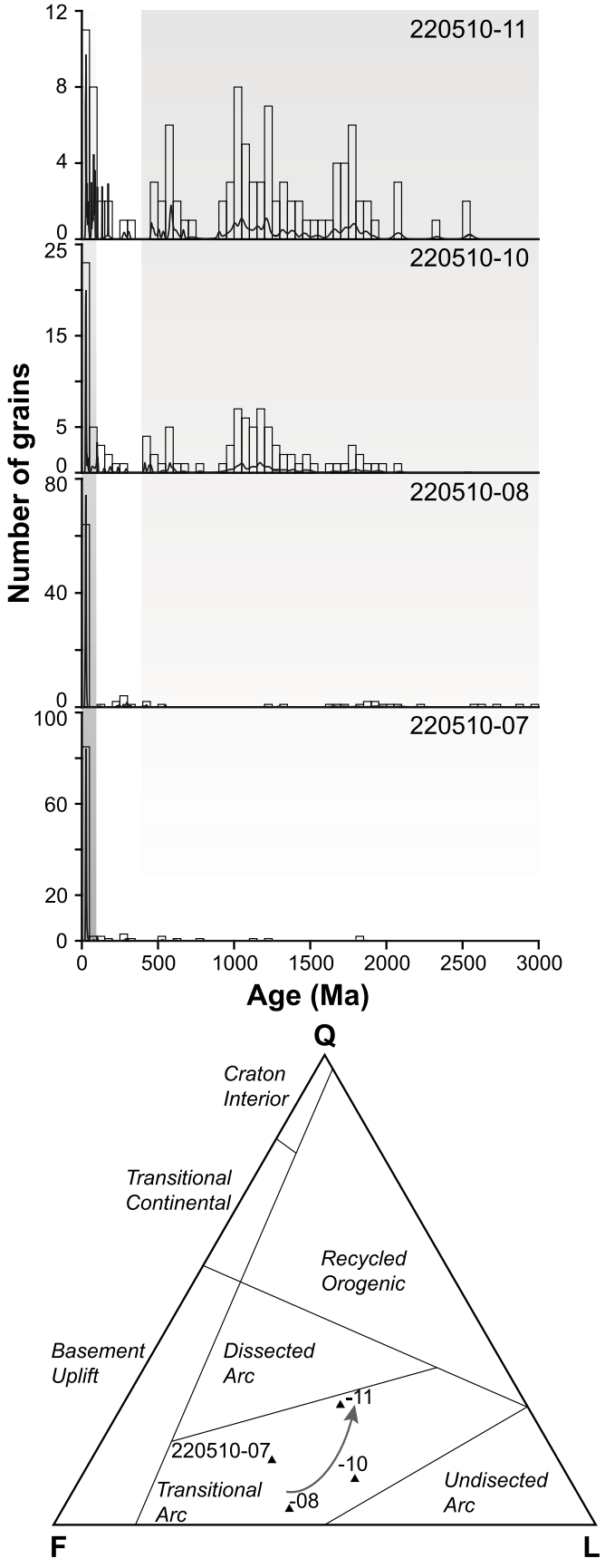

yields a U-Pb zircon age of 26.37 ± 0.68 Ma (n = 9, sample TC052).

Upsection, the next three U-Pb detrital zircon samples (240510-05, 240510-08, and 240510-10) of the lower Tinajani Formation show decreasing ages (23.51 ± 0.35, 23.2 ± 2.0, and 22.73 ± 0.72 Ma) for the youngest detrital zircon populations, in agreement with dated volcanic horizons below and within this interval. Zircon ages for tuff samples TC001 (16.92 ± 0.75 Ma, n = 17) and TC002 (16.56 ± 0.63 Ma, n = 21) provide constraints on the age of the uppermost levels of the lower Tinajani Formation at meter level ~2150.

The two stratigraphically highest sandstone samples from the uppermost exposures of the upper Tinajani Formation yield youngest grain population ages yield ages of 15.71 ± 0.97 and 17.4 ± 1.7 Ma (samples 240510-13 and TC076, respectively). The stratigraphically highest sample, TC076, is the only detrital zircon sample that does not continue the upsection trend of decreasing age of the youngest detrital zircon population. Excluding this highest sample, all of the other 14 analyzed samples yield volcanic zircon ages and young detrital zircon populations that become progressively younger upsection, suggesting that syndepositional or nearly syndepositional zircons are present in the youngest detrital zircon populations for each sample. This allows the use of both volcanic and youngest detrital zircon populations to constrain a maximum depositional age that approaches the true depositional age.

Figure 12. U-Pb detrital zircon and thin section point count analyses from four Puno Group samples taken from the Ayaviri fault growth strata outcrop located north of Ayaviri (see Figure 4b). Detrital zircon results show an upsection increase in the proportion of > 50 Ma zircons and a decrease in the number of <50 Ma zircons across the horizon preserving initial growth strata deposits. Corresponding thin section point analyses show an upsection trend from arc related toward recycled orogenic provenance.

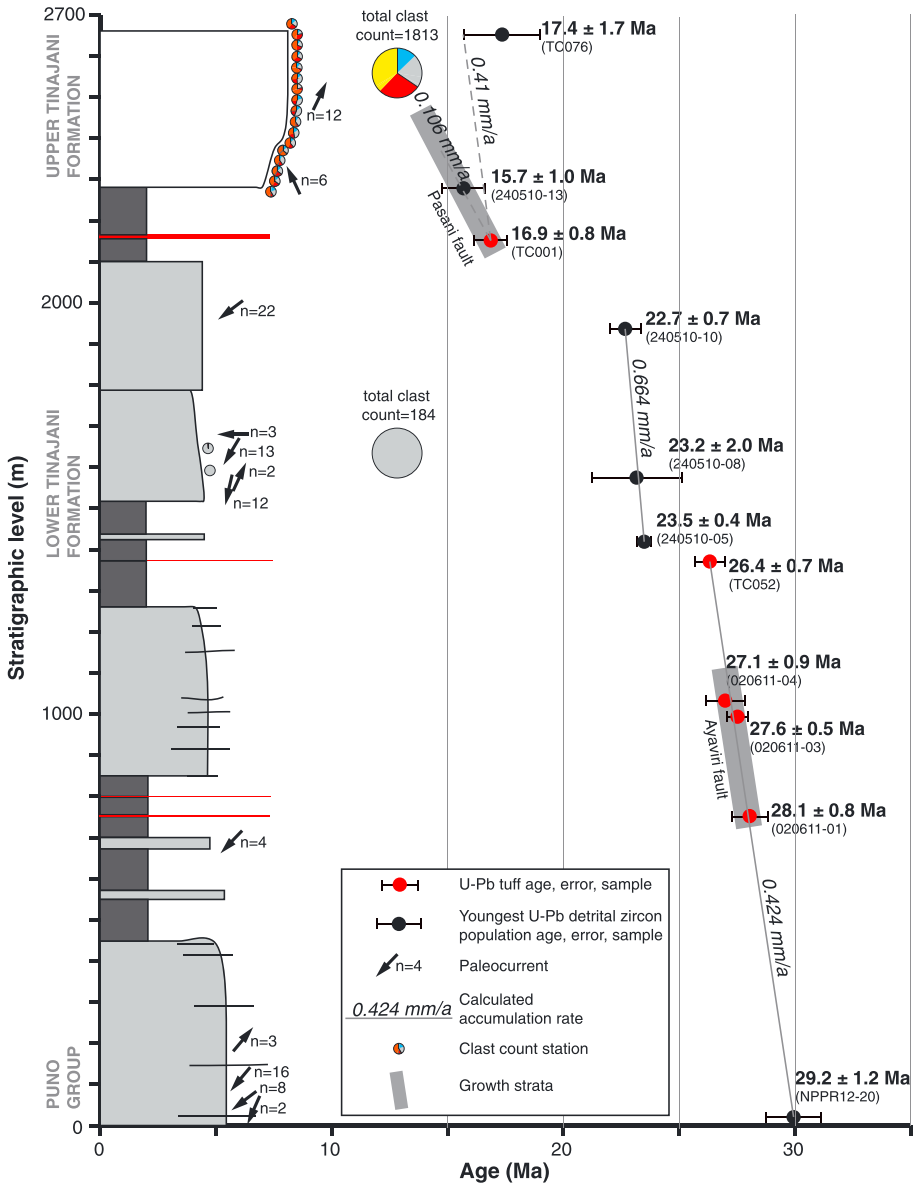

Figure 13. Generalized stratigraphic column with accumulation rates showing new isotopic age control from U-Pb zircon geochronology of sandstones (black circles) and interbedded tuffs (red circles). Small pie diagrams show clast count results by station. Large pie diagrams show average composition for multiple clast count stations. Each station is $n \approx 100$ clasts. Gray bars highlight timing of growth strata and fault motion. Arrows show paleocurrent directions. Major shifts in paleocurrents and clast composition correspond with abrupt coarsening at the ~2300 m level associated with Pasani fault growth strata.

7. Discussion

The similarities in physiographic expression between the northern and central Altiplano segments suggest a shared tectonic setting, yet debate persists regarding the style and timing of deformation and the subsidence mechanisms acting in these hinterland regions. Previous workers have suggested that the northern Altiplano was dominated by strike-slip tectonics and associated transtensional basin formation [*Carlotto*, 2013]. In the central Altiplano, shortening and thrust tectonics have been emphasized for the Cenozoic deformation and subsidence histories [*Leier et al.*, 2010]. This study focuses on the Cenozoic deformation and depositional history from the northern Altiplano. We present basin and tectonic reconstructions based on new provenance, stratigraphic, geochronologic, and structural data sets from the northern Altiplano of southern Peru (Figures 13 and 14). Patterns of provenance, subsidence, and timing of deformation suggest that the northern Altiplano, like

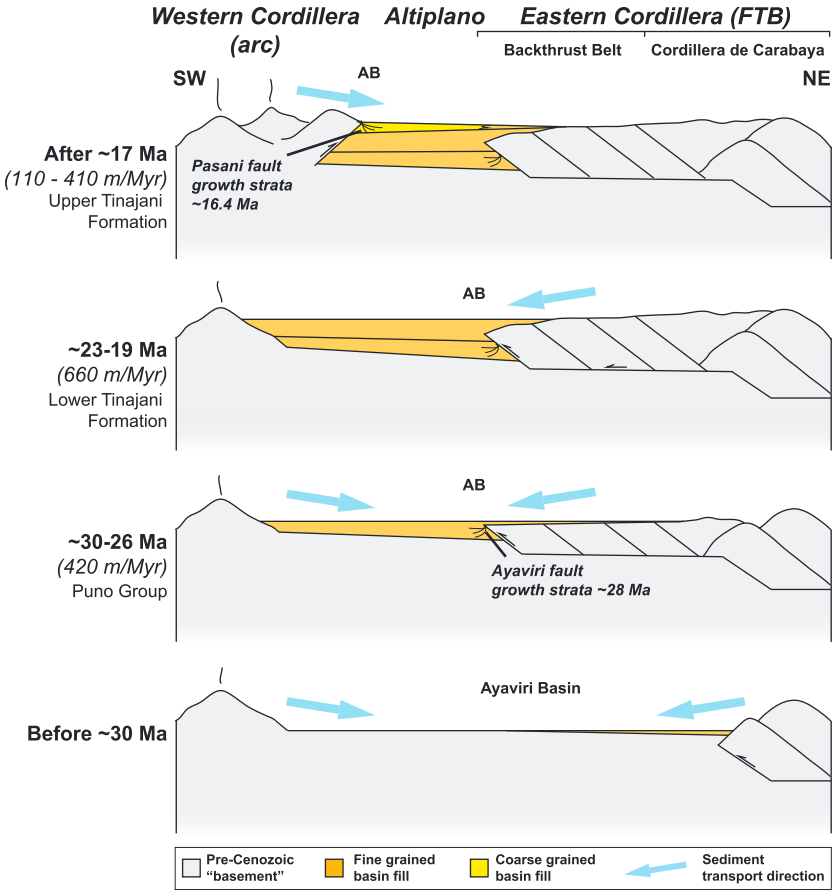

Figure 14. Schematic cross section spanning Western Cordillera, Altiplano, and Eastern Cordillera. "AB" represents Ayaviri Basin section location, and mm/yr shows subsidence rates for time interval. Before ~30 Ma, no Cenozoic preserved in this study area, although other locations have isolated Eocene-Oligocene deposits; ~30–26 Ma, shortening in the backthrust belt reaches the Ayaviri fault, creates growth strata, switches to Eastern Cordillera provenance, and initiates high subsidence rate; ~23–19 Ma, continued Eastern Cordillera provenance in sand dominated fluvial setting, continued high subsidence driven by Eastern Cordillera shortening. After ~17 Ma, Pasani fault motion created growth strata, changed to Western Cordillera provenance, and switched to coarse alluvial fan deposits.

the central Altiplano, was dominated by thrust tectonics during the late Oligocene to middle Miocene and attendant flexural subsidence in hinterland basins. We conclude that the northern and central segments of the Altiplano have a shared Cenozoic tectonic history controlled by along-strike similarities in structural geometries and kinematics (Figure 16), bolstering stratigraphic records that suggest a comparable geologic history for these hinterland regions that experienced later partitioning by out-of-sequence thrust deformation.

7.1. Basin Reconstruction

The late Oligocene Puno Group represents deposition in a sand-dominated braided fluvial system sourced from the flanking Eastern Cordillera along the northeast basin margin and from volcanic cover in the Western Cordillera. U-Pb detrital zircon samples dominated by young zircons and sandstone petrographic point counts yield sandstone compositions consistent with erosion of a volcanic-rich source. Paleocurrents, isolated pebble clasts, and Paleozoic-Proterozoic zircons support derivation of sediment consistent with exhumation of Paleozoic to Mesozoic strata found in the Eastern Cordillera. Independently, these contrasting results might be interpreted as coeval provenance from both the Western Cordillera volcanic arc and Eastern Cordillera fold-thrust belt. However, this would suggest opposing paleocurrents and complex pathways that incorporated sediment from both the Eastern and Western Cordillera, which have not been observed in the Ayaviri basin. Four key U-Pb detrital zircon samples taken from the growth strata panel preserved along the Ayaviri fault reveal the role of thrust tectonics in driving hinterland basin evolution and provenance variability (Figure 12). Sandstone compositions of these four samples suggest a transitional arc source, yet

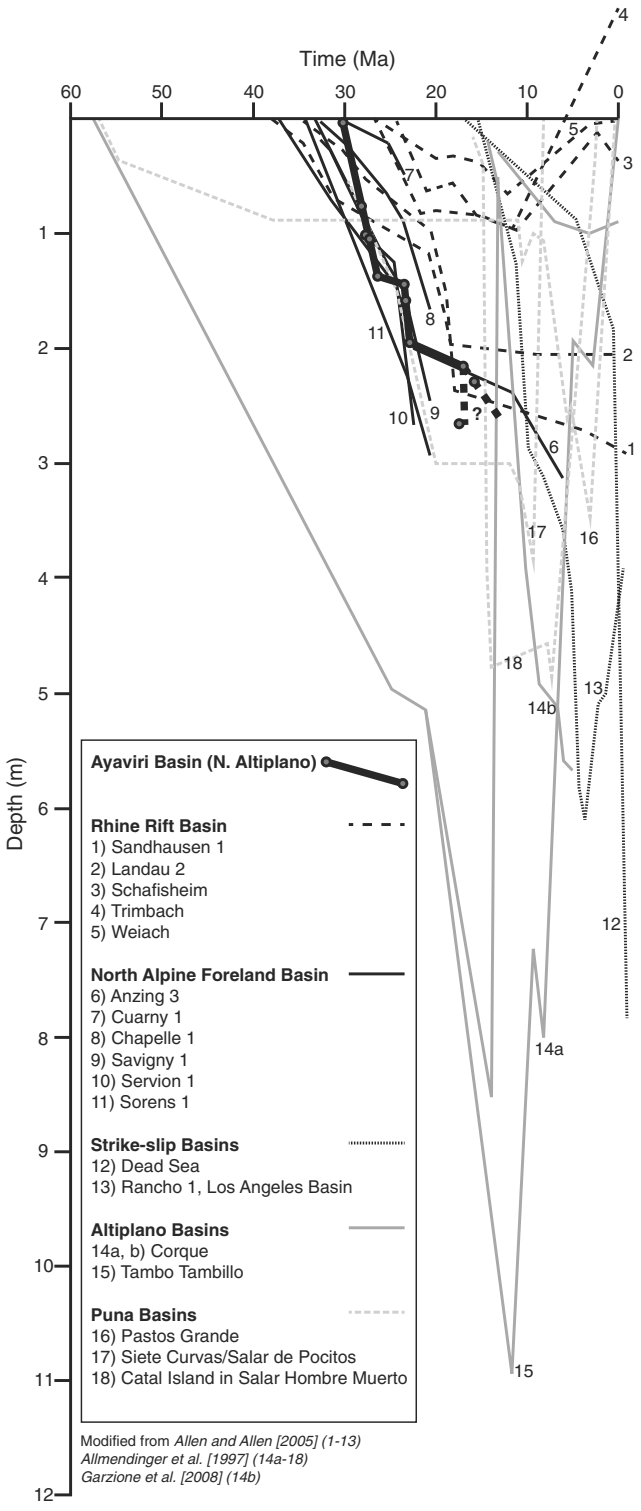

Figure 15. Comparison of the sediment accumulation history of the Ayaviri basin (thick black line) relative to foreland (thin black line), rift (dashed lines), and strike sip (dotted lines) basins [after *Allen and Allen*, 2005]. Also plotted are other Altiplano and Puna Plateau basins [after *Allmendinger et al.*, 1997]. New age control for the Ayaviri basin from U-Pb zircon ages for detrital and volcanic samples (Figure 13 for summary). The Ayaviri basin sediment accumulation rates are similar to other major Altiplano basins.

systematically trend upsection toward recycled orogenic and dissected arc sources. Accompanying detrital zircon samples reveal an upsection gradual decrease in zircons <50 Ma and an abrupt increase in Paleozoic-Proterozoic zircons across the horizon preserving initial growth strata. Young zircon populations and interbedded tuffs demonstrate deposition between 28 and 26 Ma. We suggest that these four samples from growth strata along the Ayaviri fault record a ~2 Myr provenance record where the principal sediment source changed from a Western Cordillera to Eastern Cordillera provenance due to major thrust deformation in the Eastern Cordillera and along the Ayaviri fault. The early phase of basin sedimentation appears to be governed by exhumation of the Eastern Cordillera driven by shortening along the Ayaviri fault. The Eastern Cordillera became the dominant sediment source for the northern Altiplano during the late Oligocene. Tectonic loading of the actively shortening Eastern Cordillera and thrust motion along the Ayaviri fault drove flexural subsidence during Puno Group deposition.

The early to middle Miocene lower Tinajani Formation represents continued deposition in a fluvial system, yet is generally finer grained than the Puno Group and an environment with increased anastomosing river character. U-Pb detrital zircon, sandstone petrographic point counts, paleocurrents, and conglomerate clast counts suggest continued unroofing of the Eastern Cordillera. The lower Tinajani Formation records basin fill with the highest subsidence rates from this succession, suggesting increased flexural subsidence induced by further thrust loading. We interpret that deposition of the lower Tinajani Formation was driven by flexural subsidence that resulted from continued thrust loading in the Eastern Cordillera.

The middle Miocene upper Tinajani Formation represents a shift in basin architecture driven by reverse motion along the Pasani fault. The coarse

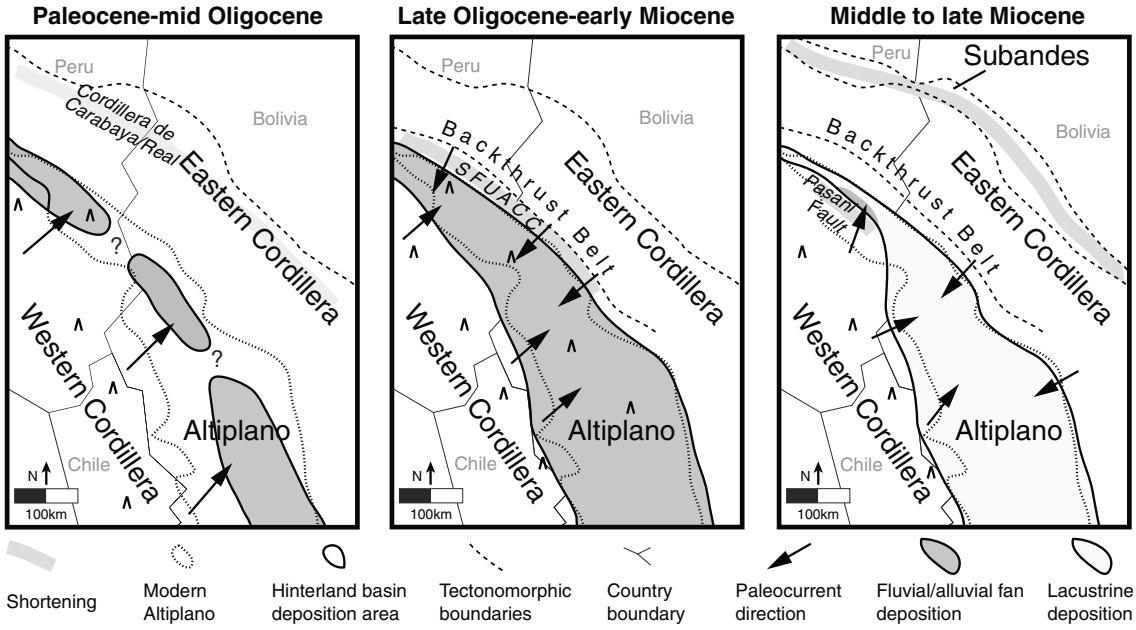

Figure 16. Proposed Altiplano scale integrated basin and deformation history. See Figure 1 for map outline. Thin gray strips represent areas of active shortening. Note the tectonomorphic zones. Eocene characterized by onset of wide-scale deposition in the Bolivian Altiplano, yet isolated or poorly preserved deposition in Peru, sourced from the Eastern Cordillera, coincident with initial widespread cooling along the Cordillera de Carabaya/Cordillera Real of Peru/Bolivia. By Oligocene, deformation propagated to the Eastern Cordillera/Altiplano boundary (SFUACC) via the Backthrust belt. Peru basins were still dominated by Eastern Cordillera sediment; Bolivian basins began receiving Western Cordillera sediment sources. In the Miocene, coeval shortening occurs in both the hinterland (out-of-sequence Pasani fault) and Subandes. Altiplano basins received sediment from a dominantly Western Cordillera source.

sandstones to boulder conglomerates of the upper Tinajani Formation were deposited in an alluvial fan environment preserved as growth strata adjacent to the actively deforming Pasani fault. U-Pb detrital zircon, conglomerate clast counts, sandstone petrographic point counts, and paleocurrents show that sediment transport was sourced in the Pasani fault hanging wall situated to the southwest of the basin. We interpret this final phase of basin subsidence as a period of reorganization in the sediment delivery pathway and provenance driven by thrust motion along the Pasani fault between 18 and 16 Ma. The Puno Group and lower Tinajani Formation were dominated by deposition of fluvial sandstones sourced from the Eastern Cordillera fold-thrust belt and Ayaviri fault, whereas the upper Tinajani Formation represents deposition in a coarse alluvial fan setting sourced from the Western Cordillera and Pasani fault hanging wall.

A simplified stratigraphic column is presented in Figure 13, and a simplified cross section spanning the northern Altiplano is presented in Figure 14. In summary, shortening along the Ayaviri fault from 28 to 26 Ma resulted in an Eastern Cordillera provenance and southwest directed sediment transport during accumulation of the Puno Group and lower Tinajani Formation. Thrusting along the Ayaviri fault also initiated rapid sedimentation. A second pulse of shortening along the Pasani fault (southwest basin margin) between 18 and 16 Ma initiated a change to Western Cordillera provenance, alluvial fan deposition, north directed sediment transport, and a second phase of rapid sedimentation.

7.2. Thrust Tectonics and Northern Altiplano Evolution

Previous workers have interpreted the Ayaviri and Pasani faults as strike-slip features that experienced either dextral or sinistral offset based on the map-view rhombohedral shape of the present-day extent of the Ayaviri basin, and on the association of fault traces with alkalinic and shoshonitic volcanic suites [*Carlier et al.*, 1996; *Mamani and Ibarra*, 2000; *Carlier et al.*, 2005; *Rousse et al.*, 2005; *Carlotto*, 2013]. On the basis of the thin-skinned thrust fault relationships, syndepositional folding, moderate fault dip, stratigraphic separation, ramp-flat cutoff variation, and systematic fault offset variation along strike, we suggest that the ~28–16 Ma history of these faults has accommodated significant reverse motion rather than strike-slip deformation. If significant strike slip deformation did occur, it must have taken place before or after the record of thrust deformation preserved along the Ayaviri and Pasani faults, in agreement with many timing estimates for vertical axis rotations in southern Peru [*Rousse et al.*, 2002, 2003; *Gilder et al.*, 2003; *Roperch et al.*, 2006].

Structural, chronostratigraphic, and provenance data sets define depositional phases for the Oligo-Miocene Ayaviri basin in the northernmost Altiplano that are temporally correlated with punctuated thrust motion along basin margin faults. Provenance records from the first phase record a major reversal during Puno Group deposition from a dominantly western (magmatic arc) to eastern (sedimentary) source area between 28 and 26 Ma, coincident with thrust activation along the Eastern Cordillera-Altiplano boundary, the Ayaviri fault. Lower Tinajani Formation preserves continued Eastern Cordillera provenance and finer-grained deposits. The last phase was also coincident with thrust motion, but along the opposing basin margin to the west, the Pasani fault. Motion along the out-of-sequence Pasani fault was coeval with a shift to Western Cordillera provenance, paleocurrent reversal, and depositional environment change between 18 and 16 Ma. The intervening time between these phases preserves limited paleosol development, lacustrine carbonate deposits, and lower sediment accumulation rates. The continuous subsidence history, record of shortening, and reorganization associated with thrust faulting preserved in the Ayaviri basin demonstrates that flexural loading from thrust deformation along the flanks of the northernmost Altiplano was the principal driver in hinterland basin initiation and evolution between ~28 and 16 Ma (Figure 14).

The sediment accumulation style and rates of the northern Altiplano suggest that it behaved as a flexural basin controlled by shortening along the basin margins. Both rapid subsidence phases record sediment accumulation rates between ~410 and 660 m/Myr, comparable to the highest rates observed in other Altiplano basins (Figure 15) [*Allmendinger et al.*, 1997; *Horton et al.*, 2001, 2002], yet preserved basin deposits are thinner than the thickest accumulations observed elsewhere in the Altiplano. Late Oligocene and middle Miocene phases of high sediment accumulation and provenance changes are coeval with Eastern Cordillera fold-thrust deformation and active Ayaviri thrust fault motion, or Pasani thrust motion, respectively. This suggests that thrust motion along basin margin faults, as evidenced by footwall syncline growth strata successions preserved along both fault traces, generated loads that were the drivers of flexural subsidence in the northern Altiplano between ~28 and 16 Ma. This interpretation is consistent with basins in the central Altiplano that also demonstrate flexural subsidence controlled by basin margin shortening.

The continuity of major structural features spanning the southern Peruvian and Bolivian Andean segments provides additional support to the interpretation of a shared geologic history in the northern and central Altiplano and the role of regional shortening in controlling central Andean tectonics. Middle to late Eocene timing constraints for initial cooling in the Eastern Cordillera are consistent along strike and have been attributed to shortening [*Farrar et al.*, 1988; *Gillis et al.*, 2006]. The backthrust belt that spans the northern and central Altiplano of southern Peru and Bolivia kinematically links deformation in the Eastern Cordillera to the Altiplano. The boundary between the Eastern Cordillera backthrust belt and the Ayaviri basin is the Ayaviri fault, part of the SFUACC. Our newly dated footwall growth strata require thrust motion along the Ayaviri fault between 28 and 26 Ma. *Sempere et al.* [1990] demonstrate deformation along the SFUACC in Bolivia at ~28–25 Ma approximately 350 km along strike suggesting deformation along this structure developed coevally throughout southern Peru and Bolivia. The along-strike continuity, synchronous activation, geometric, and kinematic similarities between the major structural features in the Peruvian and Bolivian segments of the Eastern Cordillera and Altiplano suggest a deformation history driven by regionally continuous shortening systems throughout the northern and central Altiplano (Figure 16).

New geochronologic constraints on upper crustal shortening from the northern Altiplano reveal the out-of-sequence timing of thrust deformation along the Pasani fault between 18 to 16 Ma, approximately 10 Myr younger than motion along the Ayaviri fault. The timing of Pasani fault motion may be symptomatic of a regional phase of distributed shortening [*Oncken et al.*, 2006]. Other examples of out-of-sequence thrust deformation in the Altiplano have been linked to changes in arc/slab dynamics [*Lamb*, 2011], changes in critical wedge dynamics [*McQuarrie*, 2002], and in the Puna plateau as a result of inherited crustal structures [*Strecker et al.*, 2009]. This out-of-sequence deformation in the Altiplano of Peru precedes estimates for the timing of rapid surface uplift in the Altiplano of Bolivia (~10–6 Ma) [*Garzione et al.*, 2006], Eastern Cordillera of Bolivia (after 12–9 Ma [*Barke and Lamb*, 2006]), western escarpment of the Western Cordillera of Peru (~11–8 Ma [*Schildgen et al.*, 2009a, 2009b]), shortening in the Subandes (~15 Ma [*Gillis et al.*, 2006]), arrival of conglomerates sourced from proximal sources with high relief in the Western Cordillera of Peru (~15–10 Ma [*Decou et al.*, 2011]) and is generally coeval with the proposed timing of uplift from the Western Cordillera of Peru (~19–16 Ma [*Saylor and Horton*, 2014]), and other segments of the Eastern Cordillera of Bolivia (~24–15 Ma [*Leier et al.*, 2013]). The potential geodynamic drivers for out-of-sequence upper crustal shortening in the northern Altiplano require further investigation.

8. Conclusions

1. New zircon U-Pb ages for tuff and sandstone samples constrain the depositional age of the ~2700 m Cenozoic nonmarine northern Altiplano Ayaviri hinterland basin between 29.6 ± 1.2 Ma and 15.71 ± 0.97 Ma. The Ayaviri basin is characterized by a lower ~2300 m section (Puno Group and lower Tinajani Formation) interpreted as a sand-dominated fluvial environment and an upper ~400 m section (upper Tinajani Formation) characterized by thick pebble-boulder alluvial fan conglomerates.
2. Footwall growth strata along Ayaviri and Pasani faults constrain the syndepositional timing of thrust activity along opposing basin margins at 28.1 ± 0.8 to 26.3 ± 1.6 Ma and 17.7 ± 0.8 to 16.5 ± 0.8 Ma, respectively. Ramp-flat relationships, systematic along-strike changes in stratigraphic offset, fault dip, and growth strata geometries suggest that both faults are thrusts. Deformation in the northern Altiplano was dominated by thrust tectonics between 28 and 16 Ma.
3. Basin margin thrust faults controlled sediment provenance and accumulation patterns in the northern Altiplano. New provenance data sets (U-Pb detrital zircon, paleocurrents, sandstone point counts, and clast counts) record a shift from Western Cordillera to Eastern Cordillera source in the late Oligocene coincident with Ayaviri thrust fault motion. Middle Miocene thrust motion along the Pasani fault resulted in a shift from Eastern to Western Cordillera provenance. Both phases of thrust activity were accompanied by pulses of rapid sediment accumulation at rates comparable to other Altiplano depocenters. Thrust tectonics played a major role in controlling the depositional and provenance patterns the northern Altiplano between 28 and 16 Ma.
4. The pattern of flexural subsidence and upper crustal shortening observed in the northern Altiplano is consistent with shortening tectonics proposed for the central Altiplano. The along strike continuity and coeval motion/cooling of major structural features spanning southern Peru and Bolivia suggest a shared geologic setting. The Cenozoic deformation history was driven by regionally continuous shortening systems throughout the northern and central Altiplano.
5. Geochronologic results demonstrate that thrust motion along the Pasani fault is out of sequence and may be symptomatic of distributed deformation, potentially linked to subcritical wedge dynamics, arc/slab dynamics, or surface uplift.

Acknowledgments

This research was supported by a National Science Foundation (NSF) grant (EAR-0908518), NSF Graduate Research Fellowship, ExxonMobil Geoscience Grant, Geological Society of America Graduate Student Research Grant, and support from the Jackson School of Geosciences at the University of Texas at Austin. Victor Carlotto of the Universidad Nacional San Antonio Abad del Cusco, Peru, and his students and INGEMMET associates provided critical insights regarding field sites and previous studies. We thank Nataleigh Vann for assistance in the field, Franco Prado Bedoya for logistical assistance, and the people of Ayaviri, especially Vicente Paloma, for their hospitality. Discussions with Justin Fitch, Carmala Garzione, and Ron Steel, as well as constructive comments from reviewers Victor Ramos, Andrew Leier, and Associate Editor Taylor Schildgen significantly improved the manuscript. Finally, we thank the staff of the University of Arizona LaserChron Center, as well as Joel Saylor, Ben Siks, Katie Bales, Kelly Hansard, and Alejandra Eljuri for assistance with U-Pb sample processing and LA-MC-ICPMS analyses.

References

Allen, P. A., and J. R. Allen (2005), *Basin Analysis*, 2nd ed., 549 pp., Blackwell, Mass.

Allmendinger, R. W., T. E. Jordan, S. M. Kay, and B. L. Isacks (1997), The evolution of the Altiplano-Puna plateau of the central Andes, *Annu. Rev. Earth Planet. Sci.*, *25*, 139–174.

Anadòn, P., L. Cabrera, F. Colombo, M. Marzo, and O. Riba (1986), Syntectonic intraformational unconformities in alluvial fan deposits, Eastern Ebro Basin margins (NE Spain), *Spec. Publ. Int. Assoc. Sedimentol.*, *8*, 259–271.

Aschoff, J. L., and J. G. Schmitt (2008), Distinguishing syntectonic unconformity types to enhance analysis of growth strata: An example from the Cretaceous, southeastern Nevada, U.S.A., *J. Sediment. Res.*, *78*, 608–623.

Baby, P., T. Sempere, T. Oller, L. Barrios, G. Herail, and R. Marocco (1990), Un basin en compression d'âge oligo-miocène dans le sud de l'Altiplano bolivien, *C. R. Acad. Sci.*, *311*(II), 341–347.

Bahlburg, H., J. D. Vervoort, S. A. DuFrane, V. Carlotto, C. Reimann, and J. Cardenas (2011), The U-Pb and Hf isotope evidence of detrital zircons of the Ordovician Ollantaytambo Formation, southern Peru, and the Ordovician provenance and paleogeography of southern Peru and northern Bolivia, *J. South Am. Earth Sci.*, *32*, 196–209, doi:10.1016/j.jsames.2011.07.002.

Barke, R., and S. Lamb (2006), Late Cenozoic uplift of the Eastern Cordillera, Bolivian Andes, *Earth Planet. Sci. Lett.*, *249*, 350–367, doi:10.1016/j.epsl.2006.07.012.

Barnes, J. B., T. A. Ehlers, N. McQuarrie, P. B. O'Sullivan, and J. D. Pelletier (2006), Eocene to recent variations in erosion across the central Andean fold-thrust belt, northern Bolivia: Implications for plateau evolution, *Earth Planet. Sci. Lett.*, *248*, 118–133, doi:10.1016/j.epsl.2006.05.018.

Beck, S. L., and G. Zandt (2002), The nature of orogenic crust in the central Andes, *J. Geophys. Res.*, *107*(B10), 2230, doi:10.1029/2000JB000124.

Blair, T. C., and J. G. McPherson (1994), Alluvial fans and their natural distinction from rivers based on morphology, hydraulic processes, sedimentary processes, and facies assemblages, *J. Sediment. Res.*, *A64*, 450–489.

Bonhomme, M. G., E. Audebaud, and G. Vivier (1985), Edades K-Ar de rocas hercinicas y neogenas de un perful E-W en el Peru meridional: Santiago, Chile, Departamiento Geologia, Universidad de Chile, *Comunicaciones*, *35*, 27–30.

Burbank, D. W., and J. Verges (1994), Reconstruction of topography and related depositional systems during active thrusting, *J. Geophys. Res.*, *99*, 20,281–20,297, doi:10.1029/94JB00463.

Carlier, G., J. P. Lorand, M. Bonhomme, and V. Carlotto (1996), A reappraisal of the Cenozoic Inner Arc magmatism in southern Peru: Consequences for the evolution of the Central Andes for the past 50 Ma, paper presented at 3rd International Symposium of Andean Geodynamics, Inst. de Rech. pour le Dev., Paris.

Carlier, G., J. P. Lorand, J. P. Liegeois, M. Fornari, P. Soler, V. Carlotto, and J. Cardenas (2005), Potassic-ultrapotassic mafic rocks delineate two lithospheric mantle blocks beneath the southern Altiplano, *Geology*, *33*, 601–604.

Carlotto, V. (2013), Paleogeographic and tectonic controls on the evolution of Cenozoic basins in the Altiplano and Western Cordillera of southern Peru, *Tectonophysics*, doi:10.1016/j.tecto.2013.01.002.

Carlotto, V., E. Jaillard, G. Carlier, J. Cárdenas, L. Cerpa, T. Flores, O. Latorre, and I. Ibarra (2005), Las cuencas terciarias sinorogénicas en el Altiplano y en la Cordillera Occidental del sur del Perú, in *Alberto Giesecke Matto*, vol. 6, edited by J. Arce, pp. 103–126, Sociedad Geológica del Perú, Lima.

Carroll, A. R., S. A. Graham, and M. E. Smith (2010), Walled sedimentary basin of China, *Basin Res.*, *22*, 17–32, doi:10.1111/j.1365-2117.2009.00458.x.
Clark, A. H., et al. (1990), Geologic and geochronologic constraints on the metallogenic evolution of the Andes of Southeastern Peru, *Econ. Geol.*, *85*, 1520–1583.
Coira, B., J. Davidson, C. Mpodozis, and V. A. Ramos (1982), Tectonic and magmatic evolution of the Andes of northern Argentina and Chile, *Earth Sci. Rev.*, *18*, 303–332, doi:10.1016/0012-8252(82)90042-3.
Dalmayrac, B., G. Laubacher, and R. Marocco (1980), *Geologie des Andes Peruviennes*, Travaux et Documents de L'ORSTOM, Paris.
DeCelles, P. G., and B. K. Horton (2003), Early to middle Tertiary foreland basin development and the history of Andean crustal shortening in Bolivia, *Geol. Soc. Am. Bull.*, *115*, 58–77, doi:10.1130/0016-7606(2003)115<0058:ETMTFB>2.0.CO;2.
DeCelles, P. G., M. N. Ducea, P. Kapp, and G. Zandt (2009), Cyclicity in Cordilleran orogenic systems, *Nat. Geosci.*, doi:10.1038/ngeo469.
Decou, A., H. von Eynatten, M. Mamani, T. Sempere, and G. Worner (2011), Cenozoic forearc basin sediments in Southern Peru (15–18 degrees S): Stratigraphic and heavy mineral constraints for Eocene to Miocene evolution of the Central Andes, *Sediment. Geol.*, *237*(1–2), 55–72.
Dickinson, W. R., and C. A. Suczek (1979), Plate tectonics and sandstone compositions, *Am. Assoc. Pet. Geol. Bull.*, *63*, 2164–2182.
Elger, K., O. Oncken, and J. Glodny (2005), Plateau-style accumulation of deformation: Southern Altiplano, *Tectonics*, *24,* TC4020, doi:10.1029/2004TC001675.
Ellison, R. A., B. A. Klinck, and M. P. Hawkins (1989), Deformation events in the Andean orogenic cycle in the Altiplano and Western Cordillera, southern Peru, *J. South Am. Earth Sci.*, *2*(3), 263–276.
Erslev, E. A. (1991), Trishear fault-propagation folding, *Geology*, *19*, 617–620.
Farrar, E., A. H. Clark, D. J. Kontak, and D. A. Archibald (1988), Zango-San Gaban zone: Eocene foreland boundary of the Central Andean orogen, northwest Bolivia and southeast Peru, *Geology*, *16*, 55–58.
Flores, T., and R. Rodriguez (1999), Las cuencas neogenas del sur del Peru: La cuenca Tinajani. Evolucion sedimentologica, estratigrafia, paleogeografica y tectonica (Ayaviri, Puno), Tesis de Ingeniero Geologo, UNSAAC, Cusco.
Ford, M., E. A. Williams, and A. Artoni (1997), Progressive evolution of a fault-related fold pair from growth strata geometries, Sant Llorenç de Morunys, SE Pyrenees, *J. Struct. Geol.*, *19*, 413–441.
Fornari, M., M. Mamani, I. Ibarra, and G. Carlier (2002), Datacion del periodo volcanico "Tacaza" en el Altiplano de Peru y Bolivia, paper presented at XI Congreso Peruano de Geologia, Geol. Del Peru, Lima.
Garzione, C. N., P. Molnar, J. C. Libarkin, and B. J. MacFadden (2006), Rapid late Miocene rise of the Bolivian Altiplano: Evidence for removal of mantle lithosphere, *Earth Planet. Sci. Lett.*, *241*(3–4), 543–556.
Garzione, C. N., D. J. Auerbach, J. J. S. Smith, J. J. Rosario, B. H. Passey, T. E. Jordan, and J. M. Eiler (2014), Clumped isotope evidence for diachronous surface cooling of the Altiplano and pulsed surface uplift of the Central Andes, *Earth Planet. Sci. Lett.*, *393*, 173–181.
Gehrels, G. E. (2000), Introduction to detrital zircons studies of Paleozoic and Triassic strata in western Nevada and northern California, in *Paleozoic and Triassic Paleogeography and Tectonics of Western Nevada and Northern California*, edited by M. J. Soreghan and G. E. Gehrels, *Geol. Soc. Am. Spec. Pap.*, *347*, 1–17.
Gehrels, G. E., V. A. Valencia, and J. Ruiz (2008), Enhanced precision, accuracy, efficiency, and spatial resolution of U-Pb ages by laser ablation–multicollector-inductively coupled plasma–mass spectrometry, *Geochem. Geophys. Geosyst.*, *9,* Q03017, doi:10.1029/2007GC001805.
Gilder, S., S. Rousse, D. Farber, B. McNulty, T. Sempere, V. Torres, and O. Palacios (2003), Post-Middle Oligocene origin of paleomagnetic rotations in Upper Permian to Lower Jurassic rocks from northern and southern Peru, *Earth Planet. Sci. Lett.*, *210*, 233–248, doi:10.1016/S0012-821X(03)00102-X.
Gillis, R. J., B. K. Horton, and M. Grove (2006), Thermochronology, geochronology, and upper crustal structure of the Cordillera Real: Implications for Cenozoic exhumation of the central Andean plateau, *Tectonics*, *25,* TC6007, doi:10.1029/2005TC001887.
Hampton, B. A., and B. K. Horton (2007), Sheetflow fluvial processes in a rapidly subsiding basin, Altiplano plateau, Bolivia, *Sedimentology*, *54*, 1121–1148, doi:10.1111/j.1365-3091.2007.00875.x.
Hartley, A. J., A. E. Mather, E. Jolley, and P. Turner (2005), Climatic controls on alluvial-fan activity, Coastal Cordillera, northern Chile, in *Alluvial Fans: Geomorphology, Sedimentology, Dynamics*, edited by A. M. Harvey, A. E. Mather, and M. Stokes, *Geol. Soc. London Spec. Publ.*, *251*, 95–115.
Hongn, F., C. del Papa, J. Powell, I. Petrinovic, R. Mon, V. Deraco (2007), Middle Eocene deformation and sedimentation in the Puna-Eastern Cordillera transition (23°–26°S), Control by preexisting heterogeneities on the pattern of initial Andean shortening, *Geology*, *35*, 271–274, doi:10.1130/G23189A.1.
Horton, B. K. (2012), Cenozoic evolution of hinterland basins in the Andes and Tibet, in *Tectonics of Sedimentary Basins*, 1st ed., edited by C. J. Busby and A. Azor, pp. 427–444, Blackwell, Oxford, U. K.
Horton, B. K., B. A. Hampton, and G. L. Waanders (2001), Paleogene synorogenic sedimentation in the Altiplano plateau and implications for initial mountain building in the central Andes, *Geol. Soc. Am. Bull.*, *113*, 1387–1400.
Horton, B. K., B. A. Hampton, B. N. LaReau, and E. Baldellon (2002), Tertiary provenance history of the northern and central Altiplano (Central Andes, Bolivia): A detrital record of plateau-margin tectonics, *J. Sediment. Res.*, *72*(5), 711–726.
Husson, L., and T. Sempere (2003), Thickening the Altiplano crust by gravity-driven crustal channel flow, *Geophys. Res. Lett.*, *30*(5), 1243, doi:10.1029/2002GL016877.
Ibarra, I., M. Mamani, R. Rodriguez, T. Sempere, C. Carlotto, and G. Carlier (2004), Estratigrafia y tectonica de la parte sur de la cuenca de Ayaviri, in *Nuevas Contribuciones del IRD y Sus Contrapartes al Conocimiento Geologico del sur del Peru*, *Publicacion Especial No. 5*, pp. 143–155, Institut de recherché pour le developpement, Paris.
INGEMMET (1999), Mapa Geologico del Peru, 1:1000000 scale.
Isacks, B. L. (1988), Uplift of the central Andean Plateau and bending of the Bolivian Orocline, *J. Geophys. Res.*, *93*, 3211–3231, doi:10.1029/JB093iB04p03211.
James, D. E., and I. S. Sacks (1999), Cenozoic formation of the Central Andes: A geophysical perspective, in *Geology and Ore Deposits of the Central Andes*, *Spec. Publ. no. 7*, edited by B. J. Skinner, pp. 1–25, Society of Economic Geologists, Inc, Littleton, Colo.
Jimenez, N., S. Lopez-Velasquez, and R. Santivañez (2009), Evolución tectonomagmática de los Andes Bolivianos, *Rev. Asoc. Geol. Argent.*, *65*(1), 36–67.
Jordan, T. E., and R. N. Alonso (1987), Cenozoic stratigraphy and basin tectonics of the Andes Mountains, 20°–28° south latitude, *Am. Assoc. Pet. Geol. Bull.*, *71*, 49–64.
Jordan, T. E., B. L. Isacks, R. W. Allmendinger, J. A. Brewer, V. A. Ramos, and C. J. Ando (1983), Andean tectonics related to geometry of subducted Nazca plate, *Geol. Soc. Am. Bull.*, *94*(3), 341–361.
Kay, R. W., and S. M. Kay (1993), Delamination and delamination magmatism, *Tectonophysics*, *201*, 177–189.

Kay, S. M., and B. L. Coira (2009), Shallowing and steepening subduction zones, continental lithospheric loss, magmatism, and crustal flow under the Central Andean Altiplano-Puna Plateau, in *Backbone of the Americas: Shallow Subduction, Plateau Uplift, and Ridge and Terrane Collision*, edited by S. M. Kay, V. A. Ramos, and W. R. Dickinson, *Mem. Geol. Soc. Am.*, *204*, 229–259.

Kley, J., and C. R. Monaldi (1998), Tectonic shortening and crustal thickness in the central Andes: How good is the correlation?, *Geology*, *26*, 723–726.

Kontak, D. J., A. H. Clark, E. Farrar, D. A. Archibald, and H. Baadgsgaard (1990), Late Paleozoic-early Mesozoic magmatism in the Cordillera de Carabaya, Puno, southeastern Peru: Geochronology and petrochemistry, *J. South Am. Earth Sci.*, *3*(4), 213–230.

Lamb, S. (2011), Did shortening in thick crust cause rapid Late Cenozoic uplift in the northern Bolivian Andes?, *J. Geol. Soc. London*, *168*, 1079–1092, doi:10.1144/0016-76492011-008.

LaTorre, O. O., F. Y. Oros, T. Sempered, M. Fornari, and V. Carlotto (2004), Estratigrafia y evolucion paleogena del area de Llalli - Macari (departamento de Puno), in *Nuevas Contribuciones del IRD y Sus Contrapartes al Conocimiento Geologico del Sur del Peru*, *Publicacion Especial No. 5*, pp. 143–155, Institut de Recherché Pour le Developpement, Paris.

Laubacher, G. (1978), Geologie des Andes Peruviennes, *Travaux et documents de l'ORSTOM no 95*, Paris.

Laubacher, G., and F. Mégard (1985), The Hercynian basement: A review, in *Magmatism at a Plate Edge: The Peruvian Andes*, edited by W. S. Pitcher et al., pp. 29–37, Halsted Press, New York.

Leeder, M. R. (1975), Pedogenic carbonates and flood sediment accretion rates: A quantitative model for alluvial arid-zone lithofacies, *Geol. Mag.*, *112*(3), 257–270.

Leier, A. L., N. McQuarrie, B. K. Horton, and G. E. Gehrels (2010), Upper Oligocene conglomerates of the Altiplano, central Andes: The record of deposition and deformation along the margin of a hinterland basin, *J. Sediment. Res.*, *80*, 750–762, doi:10.2110/jsr.2010.064.

Leier, A. L., N. McQuarrie, C. Garzione, and J. Eiler (2013), Stable isotope evidence for multiple pulses of rapid surface uplift in the Central Andes, Bolivia, *Earth Planet. Sci. Lett.*, *371*, 49–58.

Loewy, S. L., J. N. Connelly, and I. W. D. Dalziel (2004), An orphaned basement block: The Arequipa-Antofalla basement of the central Andean margin of South America, *Geol. Soc. Am. Bull.*, *116*, 171–187, doi:10.1130/B25226.1.

Mamani, M., and I. Ibarra (2000), Magmatismo y Tectónica Meso-Cenozoica del Altiplano y el Borde Noreste de la Cordillera Occidental de la Región de Puno, Tesis de Ingeniero Geólogo, Universidad Nacional San Antonio Abad del Cusco, 80 p.

Mamani, M., G. Worner, and T. Sempere (2010), Geochemical variations in igneous rocks of the Central Andean orocline (13 S to 18 S): Tracing crustal thickening and magma generation through time and space, *Geol. Soc. Am. Bull.*, *122*(1–2), 162–182.

Martinez, C. (1980), Structure et evolution de la chaine Hercynienne et de la chaine Andine dans la nord de la cordillera des Andes de Bolivie, *Travaux et documents de l'ORSTOM no 119*, Paris.

McBride, S., R. Robertson, and A. Clark (1983), Magmatic and metallogenetic episodes in the northern tin belt, Cordillera Real, Bolivia, *Geol. Rundsch.*, *72*(2), 685–713.

McQuarrie, N. (2002), Initial plate geometry, shortening variations, and evolution of the Bolivian orocline, *Geology*, *30*(10), 867.

McQuarrie, N., B. K. Horton, G. Zandt, S. Beck, and P. G. DeCelles (2005), Lithospheric evolution of the Andean fold–thrust belt, Bolivia, and the origin of the central Andean plateau, *Tectonophysics*, *399*, 15–37.

Mégard, F. (1984), The Andean orogenic period and its major structures in central and northern Peru, *J. Geol. Soc.*, *141*(5), 893–900.

Mégard, F., B. Dalmayrac, G. Laubacher, R. Marocco, C. Martinez, J. Paredes, and P. Tomasi (1971), La chaine Hercynienne au Perou et en Bolivie premiers resultats, *Cah. ORSTOM, Ser. Geol. III*, *1*, 5–44.

Mégard, F., D. C. Noble, E. H. McKee, and H. Bellon (1984), Multiple pulses of Neogene compressive deformation in the Ayacucho intermontane basin, Andes of central Peru, *Geol. Soc. Am. Bull.*, *95*, 1108–1117.

Miall, A. D. (1977), A review of the braided-river depositional environment, *Earth Sci. Rev.*, *13*, 1–62, doi:10.1016/0012-8252(77)90055-1.

Miall, A. D. (1978), Lithofacies types and vertical profile models in braided river deposits: A summary, in *Fluvial Sedimentology*, *Mem.*, vol. 5, Can. Soc. Pet. Geol., McAra Printing, Calgary.

Mortimer, E., B. Carrapa, I. Coutand, L. Schoenbohm, E. R. Sobel, and J. S. Gomez (2007), Fragmentation of a foreland basin in response to out-of-sequence basement uplifts and structural reactivation: El Cajon-Campo del Arenal basin, NW Argentina, *Geol. Soc. Am. Bull.*, *119*(5–6), 637–653.

Mosolf, J. G., B. K. Horton, M. T. Heizler, and R. Matos (2011), Unroofing the core of the central Andean fold-thrust belt during focused late Miocene exhumation: Evidence from the Tipuani-Mapiri wedge-top basin, Bolivia, *Basin Res.*, *23*, 346–360, doi:10.1111/j.1365-2117.2010.00491.x.

Murray, B. P., B. K. Horton, R. Matos, and M. T. Heizler (2010), Oligocene-Miocene basin evolution in the northern Altiplano, Bolivia: Implications for evolution of the central Andean backthrust belt and high plateau, *Geol. Soc. Am. Bull.*, *122*, 1443–1462, doi:10.1130/B30129.1.

Nadon, G. C. (1991), The genesis and recognition of anastomosed fluvial deposits: Data from the St. Mary river formation, southwestern Alberta, Canada, *J. Sediment. Res.*, *B64*(4), 451–463.

Nemec, W., and R. J. Steel (1984), Alluvial and coastal conglomerates: Their significant features and some comments on gravelly mass-flow deposits, in *Sedimentology of Gravels and Conglomerates*, edited by E. H. Koster and R. J. Steel, *Mem. Can. Soc. Pet. Geol.*, *10*, 1–31.

Newell, N. D. (1949), Geology of the lake Titicaca region, Peru and Bolivia, Mem. *Geol. Soc. Am.*, *36*, 111 pp.

Nijman, W., and C. Puigdefabregas (1978), Coarse-grained point bar structure in a molasse-type fluvial system, Eocene Castisent Sandstone Formation, south Pyrenean basin, in *Fluvial Sedimentology*, *Mem.*, vol. 5, pp. 487–510, Can. Soc. Pet. Geol., McAra Printing, Calgary.

Noblet, C., A. Lavenu, and R. Marocco (1996), Concept of continuum as opposed to periodic tectonism in the Andes, *Tectonophysics*, *255*, 65–78.

Oncken, O., D. Hindle, J. Kley, K. Elger, P. Victor, K. Schemmann (2006), Deformation of the Central Andean Upper Plate System – Facts, Fiction, and Constraints for Plateau Models, in *The Andes*, edited by O. Oncken et al., 3–27.

Pichavant, M., D. J. Kontak, J. Valencia Herrera, and A. H. Clark (1988), The Miocene-Pliocene Macusani volcanics, SE Peru, *Contrib. Mineral. Petrol.*, *100*, 325–338.

Platt, N. H. (1989), Lacustrine carbonates and pedogenesis: Sedimentology and origin of palustrine deposits from the Early Cretaceous Rupelo Formation, W Cameros Basin, N Spain, *Sedimentology*, *36*, 665–684.

Puigdefabregas, C., and A. Van Vliet (1978), Meandering stream deposits from the tertiary of the southern Pyrenees, in *Fluvial Sedimentology*, *Mem.*, vol. 5, Can. Soc. Pet. Geol., McAra Printing, Calgary.

Ramos, V. A. (2009), Anatomy and global context of the Andes: Main geologic features and the Andean orogenic cycle, in *Backbone of the Americas: Shallow Subduction, Plateau Uplift, and Ridge and Terrane Collision*, edited by S. M. Kay, V. A. Ramos, and W. R. Dickinson, *Mem. Geol. Soc. Am.*, *204*, 31–65.

Riba, O. (1976), Syntectonic unconformities of the Alto Cardener, Spanish Pyrenees: A genetic interpretation, *Sediment. Geol.*, *15*, 213–233.

Rochat, P., P. Baby, G. Herail, G. Mascle, O. Aranibar, and B. Colletta (1999), Genesis and kinematic of the northern Bolivian Altiplano, paper presented at 3rd International Symposium of Andean Geodynamics, Inst. de Rech. pour le Dev., Paris.

Rodriguez, R., T. Flores, and R. Marocco (1999), Analisis sedimentologico y estratigrafico de la Formacion Tinajani (Cenozoico del Altiplano del Sur del Peru). Aportes a la reconstruccion de la evolucion tectono-sedimentaria del Sur del Peru entre el Oligoceno superior y el Mioceno superior, *Bol. Soc. Geol. Peru*, *89*, 33–44.

Roeder, D., and R. L. Chamberlain (1995), Structural geology of sub-Andean fold and thrust belt in northwestern Bolivia, in *Petroleum Basins of South America*, edited by A. J. Tankard, R. Suarez Soruco, and H. J. Welsink, *Mem. AAPG*, *62*, 459–479.

Roperch, P., T. Sempere, O. Macedo, C. Arriagada, M. Fornari, C. Tapia, M. Garcia, and C. Laj (2006), Counterclockwise rotation of late Eocene–Oligocene fore-arc deposits in southern Peru and its significance for oroclinal bending in the central Andes, *Tectonics*, *25,* TC3010, doi:10.1029/2005TC001882.

Rousse, S., S. Gilder, D. Farber, B. McNulty, and V. R. Torres (2002), Paleomagnetic evidence for rapid vertical-axis rotation in the Peruvian Cordillera ca. 8 Ma, *Geology*, *30*, 75–78.

Rousse, S., S. Gilder, D. Farber, B. McNulty, P. Patriat, V. Torres, and T. Sempere (2003), Paleomagnetic tracking of mountain building in the Peruvian Andes since 10 Ma, *Tectonics, 22*(5)*,* 1048*,* doi:10.1029/2003TC001508.

Rousse, S., S. Gilder, M. Fornari, and T. Sempere (2005), Insight into the Neogene tectonic history of the northern Bolivian Orocline from new paleomagnetic and geochronologic data, *Tectonics*, *24,* TC6007, doi:10.1029/2004TC001760.

Rust, B. R. (1978), Depositional models for braided alluvium, in *Fluvial Sedimentology*, *Mem.*, vol. 5, Can. Soc. Pet. Geol., McAra Printing, Calgary.

Sandeman, H. A., A. H. Clark, and E. Farrar (1995), An integrated tectono-magmatic model for the evolution of the Southern Peruvian Andes (13-20° S) since 55 Ma, *Int. Geol. Rev.*, *37*, 1039–1073.

Saylor, J. E., and B. K. Horton (2014), Nonuniform surface uplift of the Andean plateau revealed by deuterium isotopes in Miocene volcanic glass from southern Peru, *Earth Planet. Sci. Lett.*, *387*, 120–131.

Schildgen, T. F., K. V. Hodges, K. X. Whipple, M. S. Pringle, M. van Soeste, and K. Cornell (2009a), Late Cenozoic structural and tectonic development of the western margin of the central Andean Plateau in southwest Peru, *Tectonics*, *28*, TC4007, doi:10.1029/2008TC002403.

Schildgen, T. F., T. A. Ehlers, D. M. Whipp Jr., M. C. van Soest, K. X. Whipple, and K. V. Hodges (2009b), Quantifying canyon incision and Andean Plateau surface uplift, southwest Peru: A thermochronometer and numerical modeling approach, *J. Geophys. Res.*, *114,* F04014, doi:10.1029/2009JF001305.

Sébrier, M., A. Lavenu, M. Fornari, and J. P. Soulas (1988), Tectonics and uplift in central Andes (Peru, Bolivia and northern Chile) from Eocene to present, *Geodynamique*, *3*, 85–106.

Sempere, T., G. Herail, J. Oller, and M. Bonhomme (1990), Late Oligocene–early Miocene major tectonic crisis and related basin in Bolivia, *Geology*, *18*, 946–949.

Sempere, T., G. Carlier, P. Soler, M. Fornari, V. Carlotto, J. Jacay, D. Neraudeau, J. Cardenas, S. Rosas, and N. Jimenez (2002), Late Permian-Middle Jurassic lithospheric thinning in Peru and Bolivia, and its bearing on Andean-age tectonics, *Tectonophysics*, *345*, 153–181.

Shaw, J. H., E. Novoa, and C. D. Connors (2004), Structural controls on growth stratigraphy in contractional fault-related folds, in *Thrust Tectonics and Hydrocarbon Systems*, edited by K. R. McClay, *Mem. AAPG*, *82*, 400–412.

Siks, B. C., and B. K. Horton (2011), Growth and fragmentation of the Andean foreland basin during eastward advance of fold-thrust deformation, Puna plateau and Eastern Cordillera, northern Argentina, *Tectonics*, *30*, TC6017, doi:10.1029/2011TC002944.

Smith, N. D. (1974), Sedimentology and bar formation in the upper Kicking Horse River, a braided outwash stream, *Geology*, *82*(2), 205–223.

Sobel, E. R., G. E. Hilley, and M. R. Strecker (2003), Formation of internally drained contractional basins by aridity-limited bedrock incision, *J. Geophys. Res.*, *108*(B7), 2344, doi:10.1029/2002JB001883.

Steinmann, G. (1929), *Geologie von Peru*, 448 pp., Carl Winters Universistats Buchhandlung, Heidelberg.

Strecker, M. R., R. Alonso, B. Bookhagen, B. Carrapa, I. Coutand, M. P. Hain, G. E. Hilley, E. Mortimer, L. Schoenbohm, and E. R. Sobel (2009), Does the topographic distribution of the central Andean Puna Plateau result from climatic or geodynamic processes?, *Geology*, *37*(7), 643–646.

Suppe, J., G. T. Chou, and S. C. Hook (1992), Rates of folding and faulting determined from growth strata, in *Thrust Tectonics*, edited by K. R. McClay, pp. 105–121, Chapman and Hall, London, U. K.

Tapponnier, P., X. Zhiqin, F. Roger, B. Meyer, N. Arnaud, D. Wittlinger, and Y. Jingsui (2001), Oblique stepwise rise and growth of the Tibet Plateau, *Science*, *294*, 1671–1677.

Vandervoort, D. S., T. E. Jordan, P. K. Zeitler, and R. N. Alonso (1995), Chronology of internal drainage development and uplift, southern Puna plateau, Argentine central Andes, *Geology*, *23*, 145–148, doi:10.1130/0091-7613(1995)023<0145:COIDDA>2.3.CO;2.

Vermeesch, P. (2004), How many grains are needed for a provenance study?, *Earth Planet. Sci. Lett.*, *224*, 441–451, doi:10.1016/j.epsl.2004.05.037.

Vermeesch, P. (2012), On the visualisation of detrital age distributions, *Chem. Geol.*, *312–313*, 190–194, doi:10.1016/j.chemgeo.2012.04.021.

Wells, N. A. (1984), Sheet debris flow and sheetflood conglomerates in Cretaceous cool-maritime alluvial fans, South Orkney Islands, Antarctica, in *Sedimentology of Gravels and Conglomerates*, edited by E. H. Koster and R. J. Steel, *Mem. Can. Soc. Pet. Geol.*, *10*, 133–146.

Zapata, T. R., and R. W. Allmendinger (1996), Growth stratal records of instantaneous and progressive limb rotation in the Precordillera thrust belt and Bermejo basin, Argentina, *Tectonics*, *15*, 1065–1083, doi:10.1029/96TC00431.

Erratum

In the originally published version of this article, one supporting information file was missing. The error has since been corrected and this version may be considered the authoritative version of record.